Stem Cell Reports
Article

ISSCR

OPEN ACCESS

Combined Loss of JMJD1A and JMJD1B Reveals Critical Roles for H3K9 Demethylation in the Maintenance of Embryonic Stem Cells and Early Embryogenesis

Shunsuke Kuroki,[1] Yuji Nakai,[2] Ryo Maeda,[1] Naoki Okashita,[1] Mika Akiyoshi,[3] Yutaro Yamaguchi,[3] Satsuki Kitano,[3] Hitoshi Miyachi,[3] Ryuichiro Nakato,[4] Kenji Ichiyanagi,[5] Katsuhiko Shirahige,[4] Hiroshi Kimura,[6] Yoichi Shinkai,[7] and Makoto Tachibana[1,3,*]

[1]Institute of Advanced Medical Sciences, Tokushima University, 3-18-15 Kuramoto-cho, Tokushima 770-8503, Japan
[2]Institute for Food Sciences, Hirosaki University, 2-1-1 Yanagawa, Aomori 038-0012, Japan
[3]Experimental Research Center for Infectious Diseases, Institute for Virus Research, Kyoto University, 53 Shogoin, Kawara-cho, Sakyo-ku, Kyoto 606-8597, Japan
[4]Research Center for Epigenetic Disease, The University of Tokyo, 1-1-1 Yayoi, Bonkyo-ku, Tokyo 113-0032, Japan
[5]Department of Applied Molecular Biosciences, Graduate School of Bioagricultural Sciences, Nagoya University, Furo-cho, Chikusa-ku, Nagoya 464-8601, Japan
[6]Graduate School of Bioscience and Biotechnology, Tokyo Institute of Technology, 4259 Nagatsuta, Midori-ku, Yokohama 226-8501, Japan
[7]Cellular Memory Laboratory, RIKEN Advanced Science Institute, 2-1 Hirosawa, Wako, Saitama 351-0198, Japan
*Correspondence: mtachiba@tokushima-u.ac.jp
https://doi.org/10.1016/j.stemcr.2018.02.002

SUMMARY

Histone H3 lysine 9 (H3K9) methylation is unevenly distributed in mammalian chromosomes. However, the molecular mechanism controlling the uneven distribution and its biological significance remain to be elucidated. Here, we show that JMJD1A and JMJD1B preferentially target H3K9 demethylation of gene-dense regions of chromosomes, thereby establishing an H3K9 hypomethylation state in euchromatin. JMJD1A/JMJD1B-deficient embryos died soon after implantation accompanying epiblast cell death. Furthermore, combined loss of JMJD1A and JMJD1B caused perturbed expression of metabolic genes and rapid cell death in embryonic stem cells (ESCs). These results indicate that JMJD1A/JMJD1B-meditated H3K9 demethylation has critical roles for early embryogenesis and ESC maintenance. Finally, genetic rescue experiments clarified that H3K9 overmethylation by G9A was the cause of the cell death and perturbed gene expression of JMJD1A/JMJD1B-depleted ESCs. We summarized that JMJD1A and JMJD1B, in combination, ensure early embryogenesis and ESC viability by establishing the correct H3K9 methylated epigenome.

INTRODUCTION

Posttranslational modifications in the tail region of core histones are important epigenetic marks linked to various nuclear functions, including transcriptional activity control. The discovery of enzymes that add/remove methyl groups to/from histones suggests that histone methylation levels are not statically but dynamically controlled (Kooistra and Helin, 2012). So far, individual functions of histone methyltransferases or demethylases have been studied extensively, but the role sharing between methyltransferases and demethylases for the correct establishment of histone methylated epigenome is not yet fully understood.

Histone H3 lysine 9 (H3K9) methylation is considered as an epigenetic mark of transcriptionally silenced heterochromatin. The JMJD1 family of proteins, which includes JMJD1A and its isozyme JMJD1B, reportedly possesses intrinsic H3K9 demethylating activity (Kim et al., 2012; Kuroki et al., 2013a; Yamane et al., 2006). JMJD1A plays important roles in several biological processes such as spermiogenesis (Liu et al., 2010; Okada et al., 2007), metabolism (Inagaki et al., 2009; Tateishi et al., 2009), and sex determination (Kuroki et al., 2013b). Recently, JMJD1B was shown to be required for female fertility (Liu et al., 2015). In contrast to the individual function of JMJD1A and JMJD1B in postnatal mice, the role of JMJD1 proteins in early embryogenesis and their functional redundancy are still unknown.

In this study, we demonstrated that JMJD1A and JMJD1B are redundantly but essentially required for mouse development immediately after implantation. We also demonstrated that JMJD1A and JMJD1B exhibit pivotal roles in mouse embryonic stem cell (ESC) function through the correct establishment of H3K9 methylated epigenome. Not a single depletion but depletion of both JMJD1A and JMJD1B induced a massive increase in H3K9 methylation accompanied by rapid cell death and perturbed gene expression. In control ESCs, dimethylated H3K9 (H3K9me2) was abundant in the gene-poor regions and scarce in the gene-dense regions of the chromosomes. Intriguingly, JMJD1A/JMJD1B deficiency induced a remarkable increase of H3K9me2 in the

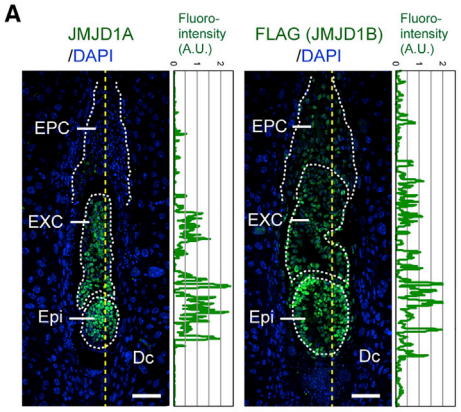

B

Jmjd1a :	+/+			+/Δ			Δ/Δ			
Jmjd1b :	+/+	+/Δ	Δ/Δ	+/+	+/Δ	Δ/Δ	+/+	+/Δ	Δ/Δ	Total
E7.5	6	9	5	7	14	13	6	10	0	70
E6.5	7	13	6	9	19	6	7	8	3#	78

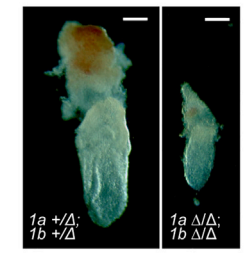

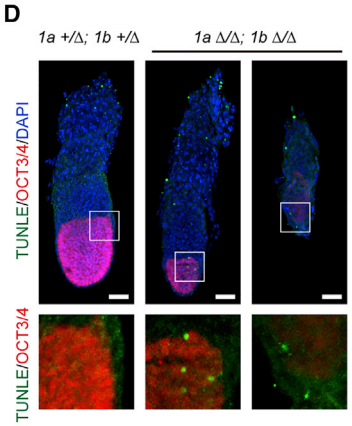

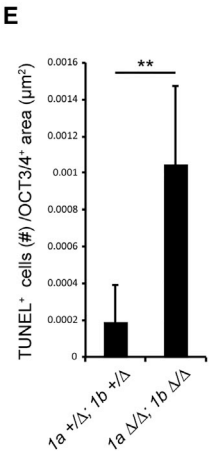

Figure 1. JMJD1A and JMJD1B Are Essential for Mouse Embryogenesis

(A) Immunofluorescence analysis of longitudinal sections of the E6.5 embryos with JMJD1A (left) and JMJD1B (right). E6.5 wild-type embryos were stained with anti-JMJD1A antibodies and DAPI (left). E6.5 *Jmjd1b*$^{+/Flag-KI}$ embryos were stained with anti-FLAG antibodies and DAPI (right). Fluorescence intensities along the dashed lines were quantified and plotted on the right side of the images. Scale bars, 100 μm. Epi, epiblast; EXC, extraembryonic ectoderm; EPC, ectoplacental cone; Dc, decidual cells. A.U., arbitrary unit.

(B) *Jmjd1a*$^{+/\Delta}$; *Jmjd1a*$^{+/\Delta}$ males and females were crossed, and the resultant embryos were genotyped at the indicated embryonic periods. *Jmjd1a*$^{\Delta/\Delta}$; *Jmjd1a*$^{\Delta/\Delta}$ embryos were found at E6.5, but not at E7.5. #, growth-retarded embryos.

(C) Gross appearances of *Jmjd1a/Jmjd1b* double-deficient embryos at E6.5 (left) when compared with a littermate control (right). *1a* and *1b* represent *Jmjd1a* and *Jmjd1b*, respectively. Scale bar, 100 μm.

(D) Whole-mount immunostaining analysis for the epiblast marker OCT3/4. Embryos were counterstained with DAPI and TUNEL to detect apoptotic cells. Scale bars, 100 μm.

(E) TUNEL-positive cells in the epiblast lineage were counted and summarized. *Jmjd1a*$^{+/\Delta}$; *Jmjd1a*$^{+/\Delta}$, n = 7; *Jmjd1a*$^{\Delta/\Delta}$; *Jmjd1a*$^{\Delta/\Delta}$, n = 3 different embryos (biological replicates). Data are presented as means ± SD. **p < 0.01 (Student's t test).

gene-dense regions, causing aberrant H3K9me2 distribution; high levels of H3K9me2 decorate chromosomes throughout. This result implies that JMJD1A/JMJD1B preferentially target H3K9 demethylation at the gene-dense euchromatin. Finally, we found that the additional mutation for an H3K9 methyltransferase G9A in a JMJD1A/JMJD1B-deficient background restored not only H3K9 overmethylation but also rapid cell death and perturbed gene expression phenotypes, indicating collaborative roles of JMJD1A/JMJD1B and G9A not only for the tuning of the H3K9 methylation levels but also for the regulation of ESC function. Taking these results together, we propose that JMJD1A/JMJD1B ensures cellular viability and transcription accuracy through the establishment of the correct H3K9 methylated epigenome in early mouse development.

RESULTS

JMJD1A and JMJD1B Are Essentially Required for Peri-implantation Development in Mice

Previous studies had demonstrated that JMJD1A and JMJD1B possess intrinsic H3K9 demethylating activity (Kim et al., 2012; Kuroki et al., 2013a; Yamane et al., 2006), suggesting that JMJD1A and JMJD1B may function in a redundant manner. To evaluate the roles of JMJD1A and JMJD1B in peri-implantation development, we examined the expression profiles of JMJD1A and JMJD1B in developing embryos (Figure 1A). Immunofluorescence analysis with anti-JMJD1A antibodies revealed that JMJD1A is expressed in the epiblast and extraembryonic ectoderm at embryonic day (E) 6.5 (Figure 1A, left). To detect the endogenous JMJD1B protein with an anti-FLAG tag antibody, we

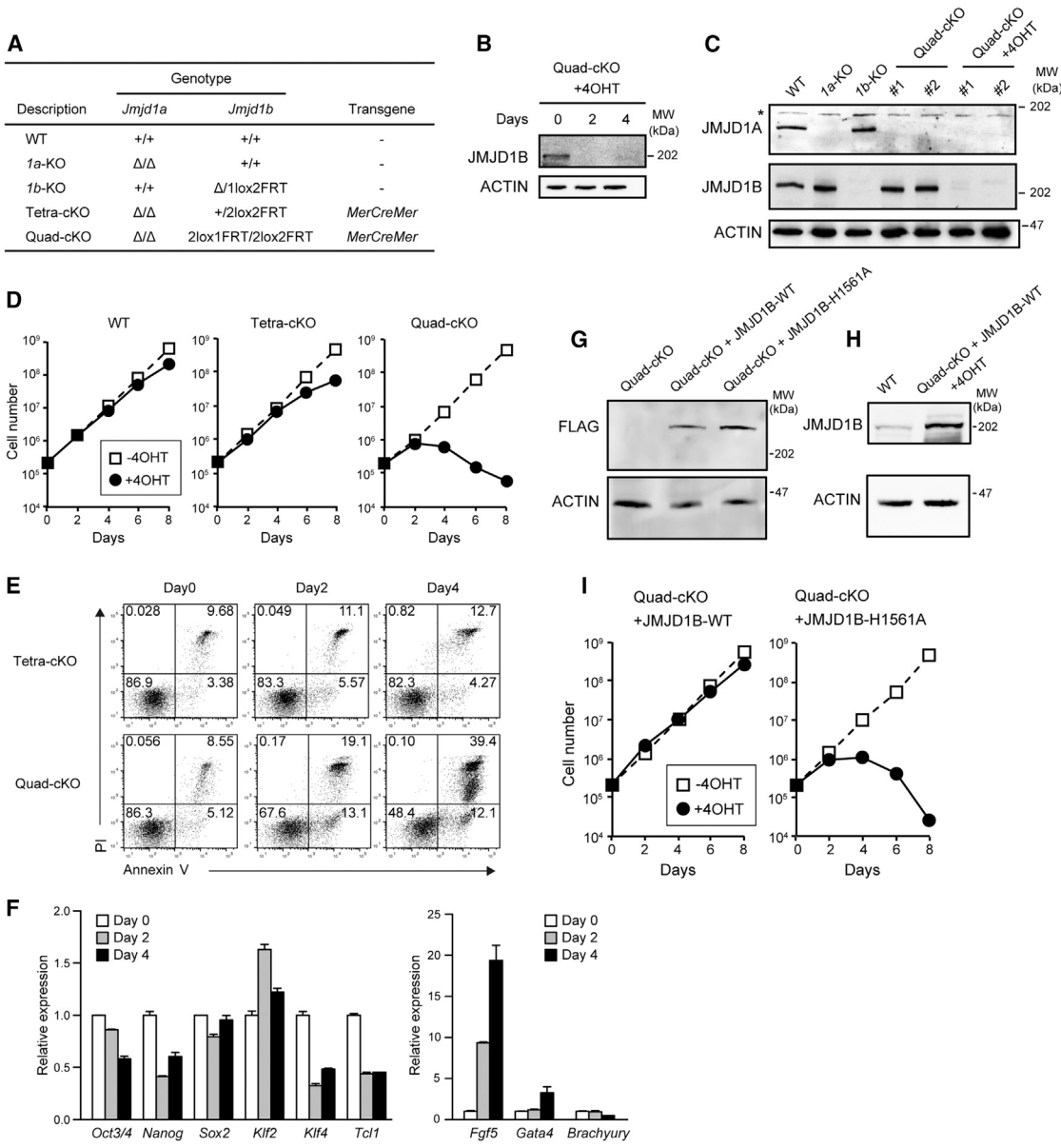

Figure 2. Depletion of JMJD1A and JMJD1B Induces Growth Arrest in ESCs

(A) List of the established ESC lines and their genotypes. MerCreMer, Cre flanked by mutated estrogen receptor ligand-binding domains.

(B) Time-course analysis of 4OHT-dependent depletion of JMJD1B in Quad-cKO cells.

(C) Immunoblot analyses of JMJD1A/JMJD1B-depleted ESC lines. Whole extracts of the indicated ESC lines were fractionated using SDS-PAGE and then applied to immunoblot analysis with antibodies against JMJD1A and JMJD1B. JMJD1A and JMJD1B were depleted in the Quad-cKO cell lines cultured with 800 nM 4OHT for 4 days. Asterisk (*) represents non-specific signals.

(D) The indicated ESC lines were cultured in the presence or absence of 4OHT. Cell numbers were determined every 2 days. Growth arrest became apparent when the Quad-cKO cell line was cultured in the presence of 4OHT for 4 days (right). In contrast, wild-type (left) and Tetra-cKO (middle) cells grew in the presence of OHT.

(E) Time-course analysis of JMJD1 depletion-induced cell death. The indicated ESC lines were cultured in the presence of 4OHT, following which the cells were stained with PI and annexin V and analyzed using flow cytometry.

(F) Expression levels of pluripotency-associated (left) and lineage-associated (right) genes in Quad-cKO cells treated with 4OHT were examined using RT-qPCR. We used *Fgf5*, *Gata4*, and *Brachyury* as the markers for primitive ectoderm, endoderm, and mesoderm, respectively. Representative data are presented from independent triplicate experiments. Error bars indicate means ± SD derived from technical replicates.

(legend continued on next page)

established knockin mouse and ESC lines carrying modified *Jmjd1b* allele (referred as *1b* hereafter). In the resultant lines, $1b^{+/Flag-KI}$ allele produces the JMJD1B protein with a carboxy-terminal FLAG tag (Figure S1). Immunofluorescence analysis of $1b^{+/Flag-KI}$ embryos with anti-FLAG tag antibody revealed that JMJD1B is expressed in the epiblast, extraembryonic ectoderm, and ectoplacental cone of E6.5 embryos (Figure 1A, right). We measured and plotted the signal intensities for JMJD1 proteins in the embryonic lineages (Figure 1A, plot analyses). Consequently, JMJD1A and JMJD1B were both found to be abundantly expressed in the epiblast of the developing embryos, indicating the potential roles of JMJD1A and JMJD1B in epiblast development.

We established mutant mice bearing the $1b^{\Delta}$ allele, which lacks exons 20–21, corresponding with a portion of the catalytic JmjC domain (Figure S1). The $1b^{\Delta/\Delta}$ mice were born at nearly the expected Mendelian ratio, but most of them died within a week after birth (Figure S2). Some of the $1b^{\Delta/\Delta}$ mice survived and developed into adults; however, their body weights were almost half those of the controls (Figure S2). These phenotypes are in accordance with those reported in a recent study (Liu et al., 2015). To evaluate the effects of compound depletion of JMJD1A and JMJD1B on mouse development, we examined postnatal animals and embryos derived from the mating of *1a*/*1b* double-heterozygous mutant mice. Among the 109 neonatal offspring, no JMJD1A/JMJD1B-deficient mice were found, strongly suggesting that JMJD1A/JMJD1B-deficient mice were embryonically lethal (Figure S2). Intriguingly, all of the mice carrying three mutant alleles of *1a* or *1b* were stillborn, indicating that the gene dosage of *1a*/*1b* is critical for prenatal development (Figure S2). Embryos bearing the *1a*/*1b* double-homozygous mutation were not found in 70 embryos at E7.5, whereas three embryos with this mutation were found in 78 embryos at E6.5 (Figure 1B). Notably, all JMJD1A/JMJD1B-deficient embryos were smaller than the controls at this stage (Figure 1C). These data suggest that JMJD1A/JMJD1B-deficient embryos display growth retardation and die around E6.5.

To examine the development of JMJD1A/JMJD1B-deficient embryos in more detail, we performed a whole-mount immunostaining analysis using antibodies against OCT3/4, which mark epiblast cells (Figure 1D). Apoptotic cells were detected by TUNEL labeling (Figure 1D). Strikingly, the mass size of OCT3/4-positive epiblasts in JMJD1A/JMJD1B-deficient embryos was smaller than those in the control embryos (Figure 1D, middle panels). We also found some JMJD1A/JMJD1B-deficient embryos without detectable epiblast cells (Figure 1D, right panels). TUNEL counterstaining analysis demonstrated a significant increase in the number of apoptotic cells in the epiblasts of JMJD1A/JMJD1B-deficient embryos (summarized in Figure 1E). These data indicate that growth retardation of JMJD1A/JMJD1B-deficient embryos can be attributed, in part, to the compromised development of the epiblast cells. We therefore conclude that JMJD1A and JMJD1B play redundant but essential roles for post-implantation development in mouse.

JMJD1A and JMJD1B Are Essentially Required for ESC Viability

To further address the roles of JMJD1-mediated H3K9 demethylation in early embryogenesis, we used mouse ESCs, which provide a good tool for studying the developmental process of pre- and post-implantation embryos. Immunoblot analysis indicated that JMJD1A and JMJD1B were both expressed in ESCs (Figure 2). We previously generated ESCs lacking JMJD1A by a simple targeting method (Inagaki et al., 2009). Also, we have established ESCs lacking JMJD1B in this study (Figure S1), indicating that neither JMJD1A nor JMJD1B is essential for ESC survival. To address the impact of JMJD1A and JMJD1B double-deficiencies in ESC function, we tried to establish an ESC line with conditionally depleted JMJD1 proteins. The conditional targeting vector of *Jmjd1b* was constructed and then introduced into the JMJD1A-deficient ESC line (Figure S1). To convert functional $1b^{2lox}$ alleles into defective $1b^{1lox}$ alleles in a 4-hydroxy tamoxifen (4OHT)-dependent manner, the MerCreMer (Cre flanked by mutated estrogen receptor ligand-binding domains) expression plasmid was also introduced into the homologous recombinant lines. We consequently obtained *1a*/*1b*-conditional knockout (KO) lines named Quad-cKO ($Jmjd1a^{\Delta/\Delta}$; $Jmjd1b^{2lox1FRT/2lox2FRT}$; *Mer-Cre-Mer*) (Figure 2A). Quad-cKO cell lines were cultured with 4OHT and then applied to immunoblot analysis (Figures 2B and 2C). Time-course

(G and H) Rescue of the growth arrest phenotype by exogenous introduction of JMJD1B into Quad-cKO cell line. (G) Expression vectors for FLAG-tagged wild-type JMJD1B or enzymatically inactive H1561A mutants of JMJD1B were individually and stably introduced into the Quad-cKO cell line. The expression levels of exogenously expressed proteins were compared by immunoblot analysis. (H) Comparison of protein expression levels of endogenously expressed JMJD1B and exogenously expressed JMJD1B using anti-JMJD1B antibody. JMJD1B expression levels were compared between wild-type ESCs and 4OHT-treated Quad-cKO cells expressing FLAG-JMJD1B-WT.

(I) Quad-cKO cell lines expressing wild-type JMJD1B (left) or the enzymatically inactive H1561A mutant of JMJD1B (right) were cultured in the presence of 4OHT. Exogenous expression of wild-type JMJD1B rescued the growth arrest phenotype of Quad-cKO cells in the presence of 4OHT, whereas the enzymatically inactive H1561A mutant did not.

experiments showed that JMJD1B signal disappeared after the 4OHT treatment for 2 days (Figure 2B). We confirmed the absence of JMJD1A signals, as well as JMJD1B signals, in the 4OHT-treated Quad-cKO cells (Figure 2C). We, thus, successfully generated ESC lines with conditionally depleted JMJD1 proteins.

Next, we examined the growth potential of Quad-cKO cell lines. Tetra-cKO (*Jmjd1a*$^{\Delta/\Delta}$; *Jmjd1b*$^{+/2lox2FRT}$; *Mer-Cre-Mer*) cells that carried two disrupted *Jmjd1a* alleles and single conditional allele of *Jmjd1b* were generated as controls (Figure 2A). The parental wild-type cells (TT2 line) and Tetra-cKO cells could grow exponentially in the presence of 4OHT (Figure 2D, left and middle panels, respectively). In contrast, when Quad-cKO cell lines were cultured in the presence of 4OHT, an increase in cell numbers was noted during the first 2 days, which was followed by a decrease in number (Figure 2D, right panel). Note that we could not establish cell lines lacking both JMJD1A and JMJD1B due to severe growth defect in the Quad-cKO cell lines when the two proteins were depleted. Taking these results together, we concluded that JMJD1A and JMJD1B are redundantly but essentially required for ESC survival.

To examine the cause of growth arrest in ESCs lacking JMJD1A and JMJD1B, we assessed the cell viability by staining with propidium iodide (PI) and annexin V (Figure 2E). The number of early apoptotic cells that stained positively with annexin V and negatively with PI increased when the Quad-cKO cell line was cultured in the presence of 4OHT for 2 days; remarkably, the number further increased with 4OHT treatment for another 2 days (Figure 2E, bottom panel). In addition, the number of dead cells that stained positively with both annexin V and PI simultaneously increased (Figure 2E, bottom panel). The progressive increase in the number of apoptotic cells might account for the growth defect of ESCs lacking JMJD1A and JMJD1B, at least in part. In contrast, 4OHT treatment had a moderate effect on the number of apoptotic and dead cells in the Tetra-cKO cell line (Figure 2E, top panel). We also conducted cell cycle analysis of Quad-cKO cells by measuring bromodeoxyuridine (BrdU) incorporation and the DNA contents (Figure S3). 4OHT treatment did not have a profound effect on cell cycle progression in both Quad-cKO and Tetra-cKO cell lines. Therefore, the growth defect phenotype in JMJD1A/JMJD1B-depleted ESCs partly results from an increase in the apoptotic cell death.

To investigate how JMJD1A/JMJD1B depletion influenced the pluripotency of ESCs, we examined mRNA expression levels of six pluripotency-associated genes (*Oct3/4*, *Nanog*, *Sox2*, *Klf2*, *Klf4*, and *Tcl1*) and three lineage-associated genes (*Fgf5*, *Gata4*, and *Brachyury*) in 4OHT-treated Quad-cKO cells (Figure 2F). The expression of four pluripotency-associated genes, *Oct3/4*, *Nanog*, *Klf4*, and *Tcl1*, was downregulated (Figure 2F, left), whereas that of the lineage-associated primitive endoderm marker gene *Fgf5* was upregulated in 4OHT-treated Quad-cKO cells (Figure 2F, right). These results indicate that JMJD1A/JMJD1B depletion in ESCs might compromise the self-renewal property of pluripotent ESCs and/or prompt their differentiation.

It is important to elucidate whether the growth arrest of JMJD1A/JMJD1B-depleted cells was dependent on JMJD1-mediated enzymatic activity. To address this issue, we performed rescue experiments using *Jmjd1b* expression vectors. Expression vectors for FLAG-tagged wild-type JMJD1B and catalytically defective JMJD1B^{H1561A} (Figure S3) were stably introduced into the Quad-cKO cells (Figure 2G). We confirmed that the protein expression levels of exogenously introduced JMJD1B were higher than that of endogenous JMJD1B (Figures 2G and 2H). As shown in Figure 2I, Quad-cKO cells carrying wild-type *Jmjd1b* transgene had a clearly restored growth potential in the presence of 4OHT. In contrast, the growth potential of Quad-cKO cells carrying *Jmjd1b*^{H1561A} transgene was not restored, even though the expression level of exogenously introduced JMJD1B^{H1561A} was higher than that of wild-type (Figure 2G). These findings indicate that the H3K9 demethylating activity of JMJD1 enzymes is absolutely required for ESC survival.

JMJD1A and JMJD1B Substantially Contribute to H3K9 Demethylation in ESCs

To address how JMJD1A and JMJD1B contribute to H3K9 methylation status of ESCs, we examined H3K9 methylation levels of mutant ESCs by immunoblot analysis (Figures 3A–3C). Dimethylated H3K9 (H3K9me2) was markedly increased in the Quad-cKO cell line when cultured in the presence of 4OHT for 2 days onward (Figure 3A). We next compared the H3K9 methylation levels among wild-type, JMJD1A-deficient, JMJD1B-deficient, and JMJD1A/JMJD1B-depleted ESCs using a panel of specific antibodies by immunoblot analysis (Figure 3B) (Kimura et al., 2008). H3K9me1 levels remained unchanged even after *1a*/*1b* compound mutation (summarized in Figure 3C, left panel). In contrast, the compound mutation led to robust increases in the levels of H3K9me2 and me3 (summarized in Figure 3C, middle and right panels, respectively). Single mutations of *1a* or *1b* led to only moderate increases in the levels of H3K9me2 and me3, indicating that JMJD1A and JMJD1B redundantly catalyze H3K9 demethylation in ESCs.

We compared nuclear distribution profiles of H3K9 methylation between wild-type and JMJD1A/JMJD1B-depleted ESCs by immunocytochemistry. Neither distribution nor intensity of H3K9me1 signals was affected by JMJD1A/JMJD1B depletion (Figure 3D). H3K9me2 signals

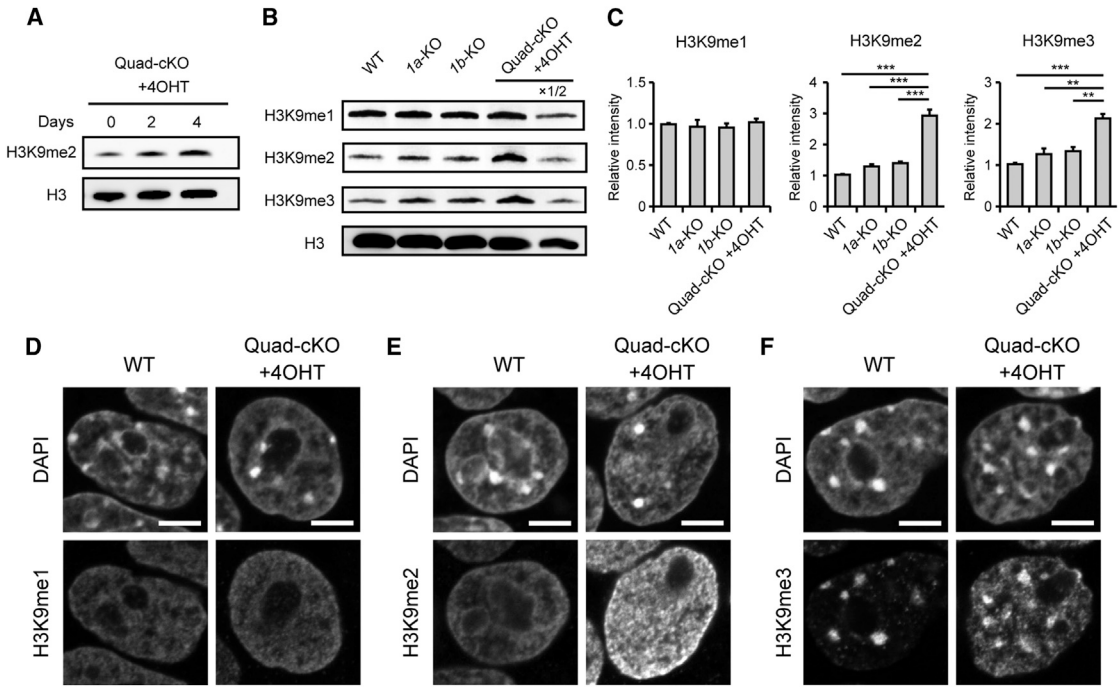

Figure 3. JMJD1A and JMJD1B Substantially Contribute to H3K9 Demethylation in ESCs

(A) Time-course analysis of JMJD1B-depletion-induced increase in H3K9me2 in 4OHT-treated Quad-cKO cells.

(B) Immunoblot analyses of H3K9 methylation levels in the indicated ESC lines.

(C) The methylation levels of H3K9me1 (left), H3K9me2 (middle), and H3K9me3 (right) in the indicated ESC lines were determined by immunoblot analysis. The intensities of H3K9me signals of wild-type cells were defined as 1. Data are presented as means ± SD (n = 3 independent experiments). **p < 0.01; ***p < 0.001 (Student's t test).

(D–F) Nuclear distribution profiles of H3K9me1 (D), H3K9me2 (E), and H3K9me3 (F) in JMJD1A/JMJD1B-depleted ESCs compared with those in the wild-type ESCs. Scale bars, 5 μm.

were detected mostly at the euchromatic regions in wild-type nuclei (Figure 3E, left panels). Distribution profiles of H3K9me2 signals seemed to be unaffected by JMJD1A/JMJD1B depletion; nevertheless, the signal intensities were dramatically increased (Figure 3E, right panels). H3K9me3 were detected mainly at the pericentric heterochromatin as dense signals in both wild-type and JMJD1A/JMJD1B-depleted cells (Figure 3F). Interestingly, we observed that JMJD1A/JMJD1B depletion led to a significant increase in H3K9me3 signals in the euchromatin (Figure 3F, right panels). These results strongly suggest that the increase in H3K9me2/3 in JMJD1A/JMJD1B-depleted ESCs is attributed to the increase in H3K9me2/3 in the euchromatin.

JMJD1A/JMJD1B-Mediated H3K9 Demethylation Targets Gene-Dense Regions of Chromosomes

The next important question is which loci are targeted by JMJD1A/JMJD1B-mediated H3K9 demethylation in ESCs. To address this issue, we performed chromatin immunoprecipitation (ChIP) analysis using antibodies against H3K9me2. Mononucleosome was prepared by enzymatic digestion of ESC chromatin and then applied to ChIP sequencing (ChIP-seq) analysis (Figure 4). Importantly, approximately 1.7 times more DNA was immunoprecipitated with anti-H3K9me2 antibody from JMJD1A/JMJD1B-depleted nuclei than from wild-type nuclei, indicating that JMJD1A/JMJD1B depletion resulted in a genome-wide increase in H3K9me2 (Figure S4). The distribution profile of H3K9me2 on chromosome 11 is representatively shown in Figure 4A; the relatively gene-poor region spans 10–50 M and relatively gene-dense region spans 50–120 M (Figure 4A, upper panel). H3K9me2 was detected throughout chromosome 11 in wild-type cells, indicating high abundance of the H3K9me2 marks (Figure 4A, middle panel). It is intriguing that H3K9me2 distributes evenly with high levels of methylation in the gene-poor region, whereas H3K9me2 distributes unevenly with high and low levels of methylation in the gene-dense region of chromosome 11 in wild-type cells. In the gene-dense region, we observed a typical feature between the gene densities and enrichment of H3K9me2 in wild-type ESCs; loci with low gene densities were heavily methylated, while those with high gene densities were hypomethylated

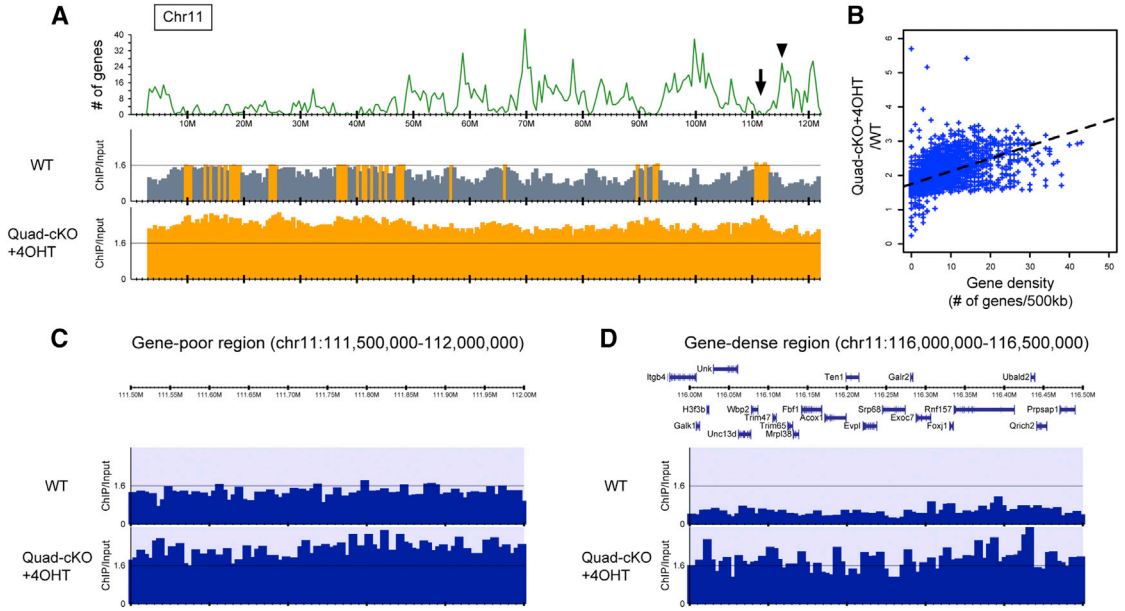

Figure 4. JMJD1A/JMJD1B-Mediated H3K9 Demethylation Targets Gene-Dense Euchromatin

(A) Distribution profiles of H3K9me2 along chromosome 11. The upper panel shows the number (#) of mm10 RefSeq genes smoothed with a width of 500 kb. The middle and lower panels represent the ratios of normalized read density between ChIP and whole-cell lysate (input) samples (ChIP/input) in wild-type and JMJD1A/JMJD1B-depleted cells (Quad-cKO+4OHT), respectively. The ratio of ChIP/input >1.6 is shown in orange.

(B) Correlation between gene density and increased H3K9me2 levels due to JMJD1A/JMJD1B depletion. The x and y axes indicate the number of mm10 RefSeq genes and the quotient of ChIP/input of Quad-cKO+4OHT divided by ChIP/input of wild-type (WT), respectively, smoothed with a 500 kb width. The dashed lines represent regression lines.

(C and D) Distribution profile of H3K9me2 in a gene-poor region (C), arrow showing the position in (A), or a gene-dense region (D), arrowhead showing the position in (A) within chromosome 11. The upper panels show the positions of the protein-coding genes, whereas lower tracks depict ChIP/input in the indicated samples.

(Figure 4A, middle panel). JMJD1A/JMJD1B depletion resulted in increased levels of H3K9me2 throughout chromosome 11 (Figure 4A, bottom panel). These characteristics were common in the other chromosomes (Figure S4). Notably, the increase in H3K9me2 levels due to JMJD1A/JMJD1B depletion in the gene-dense region seemed to be higher than that in the gene-poor region. To address this quantitatively, the relationship between the increased H3K9me2 levels due to JMJD1A/JMJD1B depletion and gene densities of all chromosomes was statistically evaluated by calculating the average levels of H3K9me2 in comparison with the gene densities (number of genes per 500 kb genome). As shown in Figure 4B, there was a positive correlation between the increased H3K9me2 levels due to JMJD1A/JMJD1B depletion and gene densities, implying that JMJD1A/JMJD1B preferentially targets H3K9 demethylation in these regions (Figure 4B). The distribution profiles of H3K9me2 with narrower windows in the gene-poor and gene-dense regions of chromosome 11 are shown in Figures 4C and 4D, respectively. In the gene-poor region, H3K9me2 levels of JMJD1A/JMJD1B-depleted cells were approximately one and a half times higher than that of wild-type cells. In contrast, H3K9me2 levels of JMJD1A/JMJD1B-depleted cells were more than three times higher than that of wild-type cells, confirming that JMJD1A/JMJD1B preferentially targets H3K9 demethylation in gene-dense regions (Figures 4C and 4D).

Profound Effect of JMJD1A/JMJD1B Depletion on Gene Expression

As the enrichment of H3K9 methylation marks is relevant to transcriptionally silenced heterochromatin, the distorted distribution of H3K9me2 might induce the alteration of gene expression in JMJD1-depleted cells. To address this, we performed a microarray analysis using RNAs from wild-type, JMJD1B-deficient, JMJD1A-deficient (Quad-cKO cell lines), and JMJD1A/JMJD1B-depleted cells (Quad-cKO cell lines cultured in the presence of 4OHT). Hierarchical clustering analysis revealed that each of the genotype-identical sets forms the smallest clusters, indicating that it is not the clonal but the genetic difference that influences gene expression (Figure 5A). The cluster of

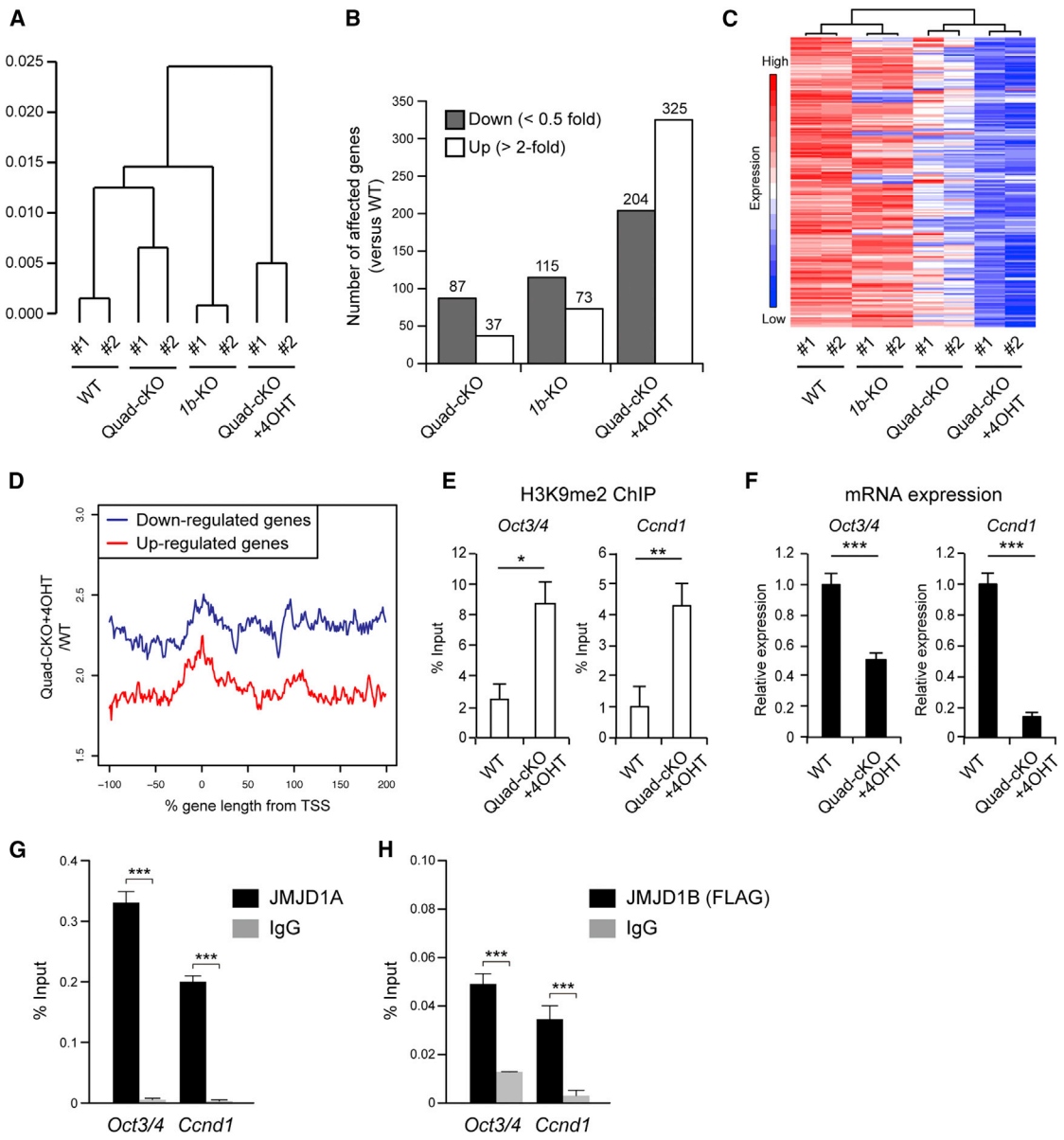

Figure 5. Depletion of JMJD1A and JMJD1B Alters Gene Expression Profile in ESCs

RNAs were prepared from ESCs and subjected to a microarray analysis using an Affymetrix mouse genome 430 2.0 array.

(A) Hierarchical clustering analysis of gene expression profiles in wild-type cells (TT2 lines), JMJD1A-deficient cells (Quad-cKO cell lines), JMJD1B-deficient cells, and JMJD1A/JMJD1B-double-depleted cells (Quad-cKO cell lines cultured with 4OHT). The farthest distance was observed between the cluster of JMJD1A/JMJD1B-double-depleted cells and the other cell clusters, indicating that the compound depletion of JMJD1A and JMJD1B has the most prominent effect on transcription.

(B) Numbers of genes affected by the JMJD1A and/or JMJD1B depletion in ESCs. Downregulated genes (<0.5-fold) and upregulated genes (>2.0-fold) due to each mutation are represented as dark and white bars, respectively.

(C) Comparison of mRNA levels in the 204 genes between the indicated samples, which were downregulated by JMJD1A/JMJD1B double depletion. Heatmap analysis demonstrated that single depletion had a moderate effect on the transcription of these genes compared with double depletion.

(D) Quantitative analysis of H3K9me2 levels of the genes regulated by JMJD1A and JMJD1B. Averaged increase in H3K9me2 around the gene bodies down- (blue) and upregulated (red) due to JMJD1A/JMJD1B depletion was plotted. The x axes indicate % gene length; 0% and 100% represent transcription start site and transcription end site, respectively. The y axes indicate the average of the quotient of ChIP/input of Quad-cKO+4OHT divided by ChIP/input of wild-type.

(legend continued on next page)

JMJD1A/JMJD1B-depleted cells was the farthest from those of the other cells, indicating that compound depletion of JMJD1A and JMJD1B has the most prominent effect on transcription. Based on this notion, the numbers of genes up- or downregulated by JMJD1A/JMJD1B double depletion were found to be larger than the numbers affected by single mutation (Figure 5B, genes are listed in Table S2).

Next, we examined the individual roles of JMJD1A and JMJD1B on the transcriptional regulation of the 204 genes that were downregulated by JMJD1A/JMJD1B double depletion. A heatmap analysis revealed that JMJD1A or JMJD1B deficiency alone had only moderate effects on the downregulation of those genes, indicating that JMJD1A and JMJD1B upregulate these genes in a redundant manner (Figure 5C). Among the 204 genes, 134 were downregulated only when both JMJD1A and JMJD1B were depleted (Figure S5). Gene ontology (GO) analyses demonstrated that metabolic processes such as one-carbon metabolism and amino acid biosynthesis were significantly enriched among the 134 genes (Figure S5). On the other hand, the genes of many pathways, such as reproductive process, inflammatory pathway, and cellular differentiation, were significantly enriched among the genes upregulated only when both JMJD1A and JMJD1B were depleted (Figure S5). To elucidate the cause of distorted gene expression in JMJD1A/JMJD1B-depleted cells, we examined H3K9 methylation levels in the genomic portion surrounding the down- and upregulated genes (Figure 5D). We found that JMJD1A/JMJD1B depletion increased H3K9 methylation levels of the downregulated genes more profoundly than those of the upregulated genes (Figure 5D). Therefore, it is conceivable that these genes are the direct targets of JMJD1A and JMJD1B.

Because previous studies have demonstrated that H3K9 methylation negatively controls the transcription of genes including *Oct3/4* (Feldman et al., 2006) and a D-type cyclin *Ccnd1* (Shirato et al., 2009), we hypothesized that JMJD1A/JMJD1B-mediated H3K9 demethylation will upregulate the transcription of *Oct3/4* and *Ccnd1*. To evaluate this hypothesis, we examined the H3K9 methylation levels of *Oct3/4* and *Ccnd1* promoters and the mRNA expression levels of *Oct3/4* and *Ccnd1* in JMJD1A/JMJD1B-depleted ESCs. As shown in Figures 5E and 5F, JMJD1A/JMJD1B depletion increased the levels of H3K9me2 at *Oct3/4* and *Ccnd1* and decreased their transcription. To further confirm the effect of JMJD1-mediated H3K9 demethylation on *Oct3/4* and *Ccnd1* regulation, we examined the enrichment of JMJD1A and JMJD1B at *Oct3/4* and *Ccnd1* loci. ChIP analysis revealed that JMJD1A was significantly enriched at the promoter regions of *Oct3/4* and *Ccnd1* in ESCs (Figure 5G). ChIP analysis of $1b^{+/\mathrm{Flag-KI}}$ ESCs demonstrated that endogenous JMJD1B was significantly enriched at the promoter regions of *Oct3/4* and *Ccnd1* (Figure 5H). Taking these results together, we conclude that JMJD1A and JMJD1B catalyze H3K9 demethylation of *Oct3/4* and *Ccnd1* gene promoters, thereby activating their transcription.

Collaborative Roles of JMJD1A/JMJD1B Demethylases and G9A Methyltransferase for Tuning the H3K9 Methylation Levels and Regulation of ESC Function

The data presented here suggest that the excess accumulation of H3K9 methylation might cause rapid cell death and perturbed gene expression in JMJD1A/JMJD1B-depleted cells. To verify this possibility, we tried to identify the enzymes responsible for H3K9 overmethylation in JMJD1A/JMJD1B-depleted cells. We have previously demonstrated that GLP/G9A methyltransferase complex catalyzes H3K9 methylation in the euchromatin (Tachibana et al., 2002, 2005). Assuming the strong candidate of this complex for euchromatic H3K9 overmethylation in the JMJD1A/JMJD1B-depleted cells, we introduced G9A-conditional alleles into the Quad-cKO cell line. Consequently, Hexa-cKO cells, in which JMJD1A, JMJD1B, and G9A could be inducibly depleted, were obtained (Figure 6A). Surprisingly, the Hexa-cKO cells demonstrated normal growth when they were cultured in the presence of 4OHT (Figure 6B), suggesting that G9A depletion restored the growth potential of JMJD1A/JMJD1B-depleted ESCs. As expected by this finding, ESC lines lacking JMJD1A, JMJD1B, and G9A (named as JGTKO) were easily established from a pool of Hexa-cKO cells cultured with 4OHT, confirming that the triple-KO ESCs have normal growth potential (Figures 6A and 6C). Next, H3K9 methylation levels of the JGTKO lines were assessed by immunoblot analysis (Figures 6D–6F). The additional *G9a* mutation induced drastic reductions in H3K9me2 and H3K9me3 levels in ESCs with JMJD1A/JMJD1B-deficient background (Figures 6E and 6F). Taken together, we conclude that G9A is a bona fide enzyme responsible for the H3K9 overmethylation in

(E) H3K9 methylation levels of the promoter regions of *Oct3/4* (left) and *Ccnd1* (right) of the indicated ESCs.
(F) mRNA expression levels of *Oct3/4* (left) and *Ccnd1* (right) of the indicated ESCs.
(G) ChIP analysis for JMJD1A at the promoter regions of *Oct3/4* (left) and *Ccnd1* (right) with anti-JMJD1A antibodies.
(H) ChIP analysis of JMJD1B at the promoter regions of *Oct3/4* (left) and *Ccnd1* (right) using anti-FLAG antibody. To detect endogenous JMJD1B with anti-FLAG antibody, we established knockin ESC line carrying $1b^{+/\mathrm{Flag-KI}}$ allele, in which the modified *1b* allele produces JMJD1B protein with a FLAG tag at its carboxy terminus (Figure S1).
For (E–H), data are presented as means ± SD from n = 3 independent experiments. *p < 0.05; **p < 0.01; ***p < 0.001 (Student's t test).

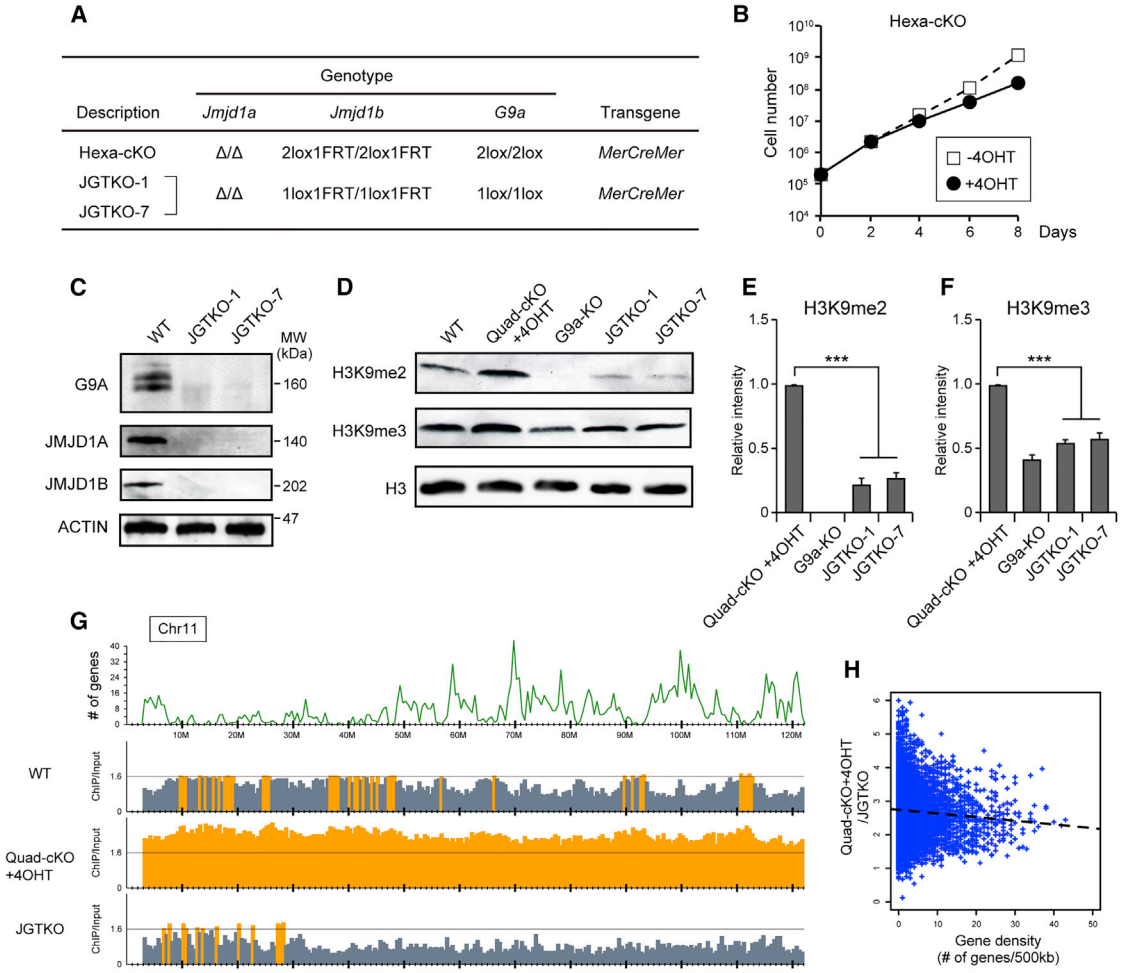

Figure 6. Collaborative Roles of JMJD1A/JMJD1B Demethylases and G9A Methyltransferase for Tuning the H3K9 Methylation Levels and Regulating ESC Function

(A) Genotypes of the established ESC line. Hexa-cKO cell line carries alleles for the null mutation of *Jmjd1a*, the conditional mutation of *Jmjd1b*, and the conditional mutation of *G9a*. ESC lines lacking JMJD1A, JMJD1B, and G9A (named JGTKO-1 and JGTKO-7) were established by cloning from a pool of Hexa-cKO cells cultured in the presence of 4OHT.

(B) Growth curve of Hexa-cKO cell line in the presence or absence of 4OHT.

(C) JMJD1A, JMJD1B, and G9A proteins were absent in JGTKO-1 and JGTKO-7 ESC lines. Whole-cell extracts were fractionated by SDS-PAGE, and then subjected to immunoblot analysis with the indicated antibodies.

(D–F) *G9a* mutation rescues the H3K9 overmethylation phenotype of JMJD1A/JMJD1B-double-depleted cells. H3K9me2 and H3K9me3 levels in the indicated cell lines were examined by immunoblot analysis (D) and summarized (E and F, respectively). The intensities of H3K9me signals of Quad-cKO + 4OHT were defined as 1. Data are presented as means ± SD from n = 3 independent experiments. ***p < 0.001 (Student's t test).

(G) Distribution profiles of H3K9me2 of JGTKO cells along chromosome 11. The top panel shows the number of mm10 RefSeq genes smoothed over 500 kb. The middle panels represent the ratios of normalized ChIP/input of ESCs of the indicated genotypes, including wild-type and JMJD1A/JMJD1B-depleted cells. The ratio of ChIP/input >1.6 is shown in orange.

(H) Correlation between gene density and decreased H3K9me2 levels due to *G9a* mutation in JMJD1A/JMJD1B-depleted cells. The x and y axes indicate the number of mm10 RefSeq genes and the quotient of ChIP/input of Quad-cKO+4OHT divided by ChIP/input of JGTKO cells, respectively, smoothed over 500 kb. Dashed lines represent regression curves.

JMJD1A/JMJD1B-depleted ESCs and that G9A-mediated H3K9 overmethylation is the cause of cell death in JMJD1A/JMJD1B-depleted ESCs.

To investigate how *G9a* mutation altered the genome-wide distribution of H3K9 methylation, we examined the H3K9me2 distribution profile of JGTKO cells by

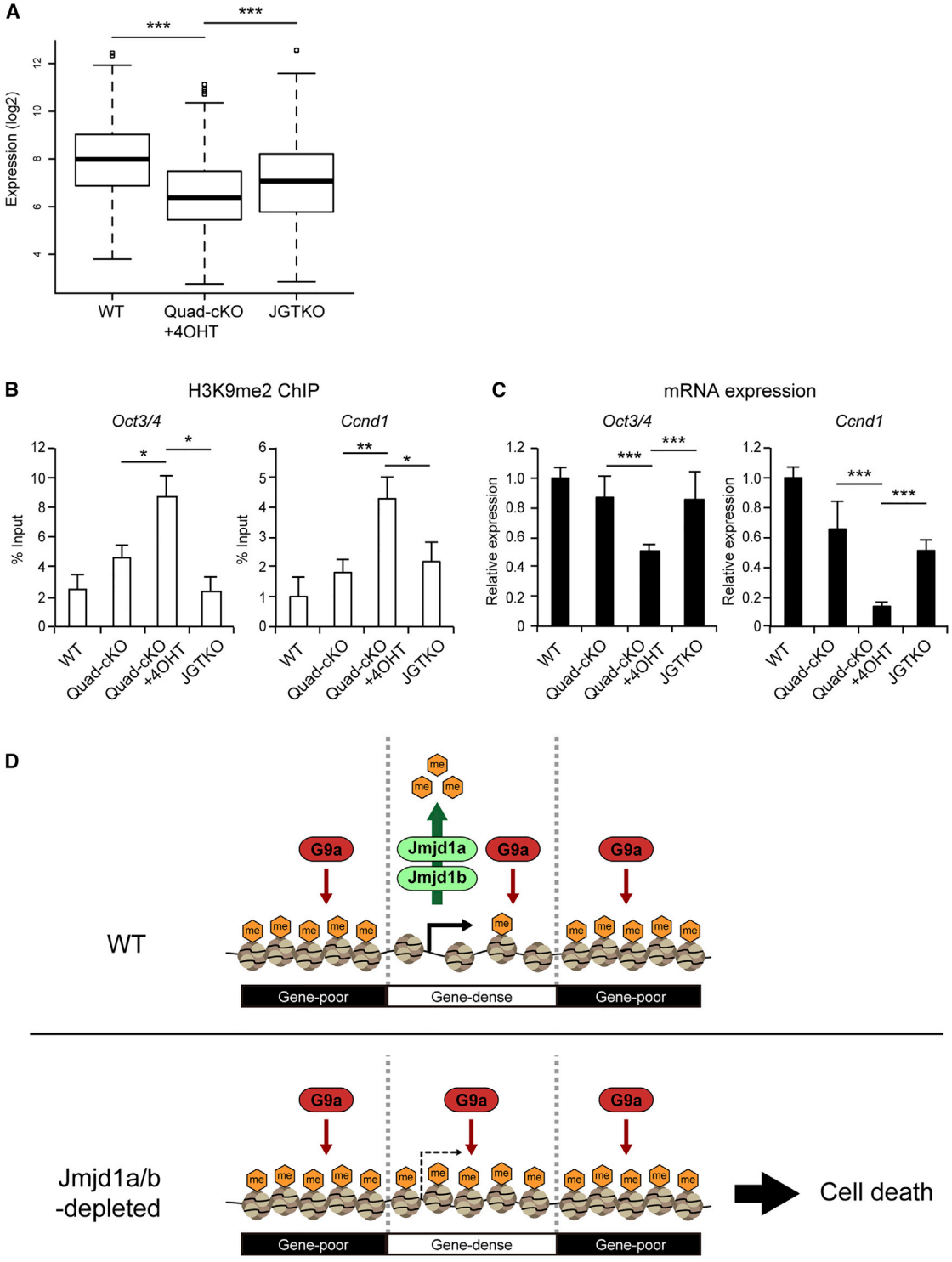

Figure 7. *G9a* Mutation Rescues JMJD1A/JMJD1B-Depletion-Induced Transcriptional Downregulation

(A) Comparison of average expression levels of 204 genes that were downregulated by JMJD1A/JMJD1B depletion between the mutant ESCs. Introduction of *G9a* mutation in JMJD1A/JMJD1B-deficient background significantly restored the expression levels of those genes. ***$p < 0.001$ (Student's t test).

(B and C) JMJD1A/JMJD1B and G9A antagonistically tune the H3K9 methylation levels of *Oct3/4* and *Ccnd1* to ensure accurate transcription. (B) The H3K9me2 levels in the promoter regions of *Oct3/4* (left) and *Ccnd1* (right) were examined by performing

(legend continued on next page)

ChIP-seq analysis (Figure 6G). Notably, less than half the amount of input DNA was immunoprecipitated with anti-H3K9me2 antibody from JGTKO cell nuclei than from JMJD1A/JMJD1B-depleted cell nuclei, indicating that G9A might actually contribute to H3K9 di-methylation in JMJD1A/JMJD1B-depleted cells (Figure S4). The distribution profile of H3K9me2 on chromosome 11 of JGTKO cells is shown in Figure 6G. We found that *G9a* mutation resulted in decreased H3K9me2 levels throughout chromosome 11, confirming that G9A substantially contributes to H3K9 di-methylation in JMJD1A/JMJD1B-depleted cells. To address the target preference of G9A-mediated H3K9 methylation, the relationship between the decreased H3K9me2 levels due to *G9a* mutation in JMJD1A/JMJD1-depleted cells and gene densities of all chromosomes was statistically evaluated as in Figure 4B. No significant differences were detected in G9A-mediated H3K9 methylation levels between the gene-poor and gene-dense regions (Figure 6H). These data suggest that the target preference of G9A-mediated H3K9 methylation is less strict than that of JMJD1A and JMJD1B-mediated H3K9 demethylation, which preferentially targets gene-dense regions (Figure 4B).

G9a Mutation Rescues JMJD1A/JMJD1B-Depletion-Induced Transcriptional Downregulation

To address the question of whether *G9a* mutation also restores gene expression profiles in JMJD1A/JMJD1B-depleted cells, we examined the expression levels of 204 genes in JGTKO cells that were downregulated due to JMJD1A/JMJD1B depletion. As shown in Figure 7A, *G9a* mutation remarkably restored the expression levels of those genes. To investigate the roles of JMJD1A/JMJD1B-mediated H3K9 demethylation and G9A-mediated H3K9 methylation in transcription regulation at single-gene level, we examined H3K9 methylation and mRNA expression of *Oct3/4* and *Ccnd1* in the serial mutant ESC lines (Figures 7B and 7C, respectively). ChIP analyses demonstrated that the elevated H3K9me2 levels were rescued by the introduction of *G9a* mutation (Figure 7B), strongly suggesting that H3K9me2 levels of *Oct3/4* and *Ccnd1* were regulated by both JMJD1A/JMJD1B-mediated H3K9 demethylation and G9A-mediated H3K9 methylation. mRNA analyses indicated typical inverse correlations between the H3K9me2 levels and the expression levels of *Oct3/4* and *Ccnd1*; the decreased mRNA expression levels of *Oct3/4* and *Ccnd1* were rescued by *G9a* mutation (Figures 7B and 7C). Thus, we conclude that the antagonistic activities between JMJD1A/JMJD1B and G9A collaboratively contribute to the tuning of H3K9 methylation levels in *Oct3/4* and *Ccnd1*. We summarize the function of JMJD1A/JMJD1B in the maintenance of ESCs as follows: H3K9 demethylases JMJD1A and JMJD1B ensure cell viability and transcriptional accuracy by removing the H3K9 methylation marks deposited by G9A in the gene-dense euchromatin (Figure 7D).

As shown in Figure 6B, JMJD1A/JMJD1B- and G9A-triple-KO cells clearly re-acquired growth potential, indicating that ESCs can survive in the absence of JMJD1A/JMJD1B- and G9A-mediated H3K9 methylation tuning. To address the possible importance of JMJD1A/JMJD1B- and G9A-mediated H3K9 methylation tuning for differentiation of ESCs, we cultured the JMJD1A/JMJD1B/G9A-triple-deficient JGTKO-1 line under differentiating condition without leukemia inhibitory factor. As shown in Figure S6, the JGTKO cell line immediately lost growth potential in the differentiating condition. We further examined the kinetics of mRNA expression of several pluripotency-associated genes (Figure S6). In wild-type cells, pluripotency-associated genes were downregulated concomitantly with differentiation. In contrast, some pluripotency-associated genes were not downregulated in the JGTKO line in the differentiating condition (Figure S6). These results indicate that collaborative H3K9 methylation tuning by JMJD1A/JMJD1B and G9A plays an indispensable role in the suppression of pluripotency-associated genes when ESCs undergo differentiation.

DISCUSSION

We previously demonstrated that JMJD1A and JMJD1B have intrinsic enzymatic activities for H3K9 demethylation (Kuroki et al., 2013a). Here, we report the functional overlap of JMJD1A and JMJD1B in early embryogenesis and ESC maintenance in mice. As expected, JMJD1A and JMJD1B

ChIP-qPCR analyses. Increased H3K9me2 levels in these genes in JMJD1A/JMJD1B-double-depleted cells were rescued by G9A depletion. (C) The expression levels of *Oct3/4* (left) and *Ccnd1* (right) were examined by RT-qPCR analyses. Reduced expression levels of these genes in JMJD1A/JMJD1B-double-depleted cells were rescued by G9A depletion. mRNA expression levels of wild-type cells were defined as 1. For (B) and (C), data are presented as means ± SD. n = 3 independent experiments. *p < 0.05; **p < 0.01; ***p < 0.001 (Student's t test).

(D) Schematic representation of the roles of JMJD1A/JMJD1B in ESCs. JMJD1A/JMJD1B ensure cell viability and transcriptional accuracy by antagonizing G9a-mediated H3K9 overmethylation in gene-rich euchromatin in ESCs. In wild-type ESCs, JMJD1A/JMJD1B preferentially remove H3K9 methylation marks from gene-rich euchromatin. The compound loss of JMJD1A/JMJD1B results in G9a-mediated H3K9 overmethylation in euchromatin, thereby inducing cell death and impaired gene expression.

are both expressed in developing embryos and ESCs (Figures 1 and 2, respectively). On the other hand, *Jmjd1a* single-mutant mice display unique phenotypes, such as defects of spermiogenesis (Liu et al., 2010; Okada et al., 2007), metabolism (Inagaki et al., 2009; Tateishi et al., 2009), and sex determination (Kuroki et al., 2013b). We speculate that *Jmjd1a* is highly expressed in these tissues and therefore plays a dominant role in H3K9 demethylation. According to this notion, protein expression profiles of JMJD1A and JMJD1B are distinctive in the human tissues (http://www.humanproteomemap.org/).

We demonstrated that the combined depletion of JMJD1A and JMJD1B has a synergistic effect on gene expression (Figure 5). It is plausible that the growth defect phenotype of JMJD1A/JMJD1B-depleted ESCs is attributed to distorted gene expression, at least partly. Note that the GO terms for the multiple metabolic pathways downregulated by JMJD1A/JMJD1B deficiency include the one-carbon and amino acid biosynthetic pathways (Figure S5). It is feasible that disorders in multiple metabolic pathways might induce the loss of ESC viability.

Mammalian cells have multiple H3K9 methyltransferases and demethylases with different product/substrate specificities and target specificities (Greer and Shi, 2012; Kooistra and Helin, 2012). The antagonistic activities of H3K9 methyltransferase and demethylase are considered to contribute to the tuning of the H3K9 methylation levels, but how and which combination of methyltransferase/demethylase contributes to this regulation were still unresolved. Here, we demonstrated that JMJD1A/JMJD1B demethylases and G9A methyltransferase are involved in the tuning of the H3K9 methylation levels (summarized in Figure 7D). To the best of our knowledge, this is the first study revealing the role sharing between demethylase and methyltransferase for the correct establishment of histone methylated epigenome. In this context, G9A-mediated H3K9 methylation seems to exhibit less specificity for the target region of chromosomes (Figure 6H). According to this notion, a previous ChIP-seq analysis demonstrated that G9A is located in almost all chromosomal regions (Mozzetta et al., 2014). On the other hand, ChIP-seq analysis in our present study revealed that JMJD1A/JMJD1B-mediated H3K9 demethylation may preferentially target gene-dense euchromatin (Figure 4B). How JMJD1A/JMJD1B exerts target specificity toward euchromatin needs to be ascertained. Like most of the histone modification enzymes, JMJD1A and JMJD1B do not contain typical DNA recognition motifs, strongly suggesting that the target specificity of these proteins is dependent on the interaction of other proteins. JMJD1A and JMJD1B bear the signature LXXLL motif indicative of a protein-protein interaction with the nuclear receptors. It was reported that JMJD1A is recruited to androgen-receptor target genes in a hormone-dependent manner (Yamane et al., 2006). A recent study revealed that phosphorylation of JMJD1A strengthens the binding capacity to binding partner proteins, such as PPARγ (Abe et al., 2015). However, as shown in Figure 4D, it seems likely that JMJD1A/JMJD1B-mediated H3K9 demethylation can target megabase ranges of the chromosomal region. Thus, it is also conceivable that JMJD1A/JMJD1B forms a complex with a nuclear protein, which can recognize the global chromatin structure rather than specific DNA sequences.

Unexpectedly, our results indicate that JMJD1A/JMJD1B- and G9A-mediated H3K9 methylation tuning is dispensable for the maintenance of ESCs (Figure 6B). On the other hand, this tuning machinery seems to play an indispensable role when ESCs undergo differentiation because the downregulation of pluripotency-associated genes was compromised in the JGTKO line when cultured in the differentiating condition (Figure S6). A previous study demonstrated that the forced expression of protein kinase A in ESCs induces cellular differentiation concomitantly with G9A-mediated H3K9 methylation of the *Oct3/4* locus (Yamamizu et al., 2012). We demonstrated that the *Oct3/4* locus undergoes not only G9A-mediated H3K9 methylation but also JMJD1A/JMJD1B-mediated H3K9 demethylation to ensure correct expression levels (Figures 7B and 7C). It is plausible that the collaboration of JMJD1A/JMJD1B-mediated H3K9 demethylation and G9A-mediated H3K9 methylation may be essentially required for the rearrangement of H3K9 methylated epigenome upon differentiation. Based on the result that *G9a* mutation rescued compromised gene expression due to JMJD1A/JMJD1B depletion (Figure 7A), we speculate that the fine-tuning of H3K9 methylation by JMJD1 and G9A may contribute to transcriptional regulation of not only *Oct3/4* but also other genes important for ESC function.

It has been demonstrated that lysine methyltransferases and demethylases regulate methylation dynamics not only for histones but also for non-histone proteins (Hamamoto et al., 2015). Most recently, it was demonstrated that the GLP/G9A complex methylates lysine residues within the TARK motif of DNA Ligase 1, which is similar to the H3K9 methylation within the TARK motif of histone H3 (Ferry et al., 2017). To the best of our knowledge, the contribution of JMJD1A and JMJD1B toward the demethylation of non-histone protein substrates has not been reported. The possibility that JMJD1A/JMJD1B and G9A regulate methylation of non-histone proteins warrants further investigation.

Note that the levels of H3K9me2 and H3K9me3 in the triple-KO cells were slightly but significantly higher than those in the *G9a*-deficient cells (Figures 6D–6F). These data indicate that JMJD1A and JMJD1B demethylate the H3K9me2 and H3K9me3 marks deposited by H3K9 methyltransferase(s) other than G9A. We propose that the

balance in H3K9 methylation levels is maintained in a highly orchestrated manner, governed by multiple enzymes for methylation and demethylation.

EXPERIMENTAL PROCEDURES

Generation of Mutant Mice and ESCs

Serial knockin targeting vectors were constructed by the bacterial artificial chromosome recombineering technique (Copeland et al., 2001) and then introduced into the ESC line TT2. Detailed information for the generation of mutant mice and ESCs is described in Supplemental Information. All animal experiments were performed under the animal ethical guidelines of Tokushima University (experiment number 14,108, approved by The Ethics Committee of Tokushima University for Animal Research) and Kyoto University (experiment number A12-6-2, approved by Animal Experimentation Committee of Kyoto University).

ACCESSION NUMBERS

The accession numbers for the microarray data and the ChIP-seq data reported in this paper are GEO: GSE98761 and DDBJ: DRA006496, respectively.

SUPPLEMENTAL INFORMATION

Supplemental Information includes Supplemental Experimental Procedures, six figures, and two tables and can be found with this article online at https://doi.org/10.1016/j.stemcr.2018.02.002.

AUTHOR CONTRIBUTIONS

S. Kuroki and M.T. designed experiments. S. Kuroki, Y.N., R.M., N.O., M.A., Y.Y., S. Kitano, H.M., R.N., K.I., K.S., and M.T. performed experiments and analyzed data. H.K. and Y.S. provided resources. S. Kuroki and M.T. wrote the paper.

ACKNOWLEDGMENTS

We are grateful to Hiroyuki Sasaki (Kyushu University) and Naoko Yokota (Tokyo University) for support during the *in silico* analysis. We also thank Enago for the English language review. We are especially grateful to Toru Nakano for critical reading of the manuscript. We thank all members of the Tachibana laboratory. This work was supported by JSPS KAKENHI grant numbers JP26250037 (M.T.), JP16H01218 (M.T.), JP16H01409 (M.T.), and JP16K21196 (S. Kuroki); the Funding Program for Next Generation World-Leading Researchers (M.T.); the Takeda Science Foundation (M.T. and S. Kuroki); the Suntory Foundation for Life Sciences (S. Kuroki); and a Promotion of Science Cooperative Research Grant of the Institute for Enzyme Research, Joint Usage/Research Center, Tokushima University (H.M.).

Received: September 3, 2017
Revised: February 6, 2018
Accepted: February 7, 2018
Published: March 8, 2018

REFERENCES

Abe, Y., Rozqie, R., Matsumura, Y., Kawamura, T., Nakaki, R., Tsurutani, Y., Tanimura-Inagaki, K., Shiono, A., Magoori, K., Nakamura, K., et al. (2015). JMJD1A is a signal-sensing scaffold that regulates acute chromatin dynamics via SWI/SNF association for thermogenesis. Nat. Commun. *6*, 7052.

Copeland, N.G., Jenkins, N.A., and Court, D.L. (2001). Recombineering: a powerful new tool for mouse functional genomics. Nat. Rev. Genet. *2*, 769–779.

Feldman, N., Gerson, A., Fang, J., Li, E., Zhang, Y., Shinkai, Y., Cedar, H., and Bergman, Y. (2006). G9a-mediated irreversible epigenetic inactivation of Oct-3/4 during early embryogenesis. Nat. Cell Biol. *8*, 188–194.

Ferry, L., Fournier, A., Tsusaka, T., Adelmant, G., Shimazu, T., Matano, S., Kirsh, O., Amouroux, R., Dohmae, N., Suzuki, T., et al. (2017). Methylation of DNA ligase 1 by G9a/GLP recruits UHRF1 to replicating DNA and regulates DNA methylation. Mol. Cell *67*, 550–565.e5.

Greer, E.L., and Shi, Y. (2012). Histone methylation: a dynamic mark in health, disease and inheritance. Nat. Rev. Genet. *13*, 343–357.

Hamamoto, R., Saloura, V., and Nakamura, Y. (2015). Critical roles of non-histone protein lysine methylation in human tumorigenesis. Nat. Rev. Cancer *15*, 110–124.

Inagaki, T., Tachibana, M., Magoori, K., Kudo, H., Tanaka, T., Okamura, M., Naito, M., Kodama, T., Shinkai, Y., and Sakai, J. (2009). Obesity and metabolic syndrome in histone demethylase JHDM2a-deficient mice. Genes Cells *14*, 991–1001.

Kim, J.Y., Kim, K.B., Eom, G.H., Choe, N., Kee, H.J., Son, H.J., Oh, S.T., Kim, D.W., Pak, J.H., Baek, H.J., et al. (2012). KDM3B is the H3K9 demethylase involved in transcriptional activation of lmo2 in leukemia. Mol. Cell Biol. *32*, 2917–2933.

Kimura, H., Hayashi-Takanaka, Y., Goto, Y., Takizawa, N., and Nozaki, N. (2008). The organization of histone H3 modifications as revealed by a panel of specific monoclonal antibodies. Cell Struct. Funct. *33*, 61–73.

Kooistra, S.M., and Helin, K. (2012). Molecular mechanisms and potential functions of histone demethylases. Nat. Rev. Mol. Cell Biol. *13*, 297–311.

Kuroki, S., Akiyoshi, M., Tokura, M., Miyachi, H., Nakai, Y., Kimura, H., Shinkai, Y., and Tachibana, M. (2013a). JMJD1C, a JmjC domain-containing protein, is required for long-term maintenance of male germ cells in mice. Biol. Reprod. *89*, 93.

Kuroki, S., Matoba, S., Akiyoshi, M., Matsumura, Y., Miyachi, H., Mise, N., Abe, K., Ogura, A., Wilhelm, D., Koopman, P., et al. (2013b). Epigenetic regulation of mouse sex determination by the histone demethylase Jmjd1a. Science *341*, 1106–1109.

Liu, Z., Chen, X., Zhou, S., Liao, L., Jiang, R., and Xu, J. (2015). The histone H3K9 demethylase Kdm3b is required for somatic growth and female reproductive function. Int. J. Biol. Sci. *11*, 494–507.

Liu, Z., Zhou, S., Liao, L., Chen, X., Meistrich, M., and Xu, J. (2010). Jmjd1a demethylase-regulated histone modification is essential for cAMP-response element modulator-regulated gene expression and spermatogenesis. J. Biol. Chem. *285*, 2758–2770.

Mozzetta, C., Pontis, J., Fritsch, L., Robin, P., Portoso, M., Proux, C., Margueron, R., and Ait-Si-Ali, S. (2014). The histone H3 lysine 9 methyltransferases G9a and GLP regulate polycomb repressive complex 2-mediated gene silencing. Mol. Cell *53*, 277–289.

Okada, Y., Scott, G., Ray, M.K., Mishina, Y., and Zhang, Y. (2007). Histone demethylase JHDM2A is critical for Tnp1 and Prm1 transcription and spermatogenesis. Nature *450*, 119–123.

Shirato, H., Ogawa, S., Nakajima, K., Inagawa, M., Kojima, M., Tachibana, M., Shinkai, Y., and Takeuchi, T. (2009). A jumonji (Jarid2) protein complex represses cyclin D1 expression by methylation of histone H3-K9. J. Biol. Chem. *284*, 733–739.

Tachibana, M., Sugimoto, K., Nozaki, M., Ueda, J., Ohta, T., Ohki, M., Fukuda, M., Takeda, N., Niida, H., Kato, H., et al. (2002). G9a histone methyltransferase plays a dominant role in euchromatic histone H3 lysine 9 methylation and is essential for early embryogenesis. Genes Dev. *16*, 1779–1791.

Tachibana, M., Ueda, J., Fukuda, M., Takeda, N., Ohta, T., Iwanari, H., Sakihama, T., Kodama, T., Hamakubo, T., and Shinkai, Y. (2005). Histone methyltransferases G9a and GLP form heteromeric complexes and are both crucial for methylation of euchromatin at H3-K9. Genes Dev. *19*, 815–826.

Tateishi, K., Okada, Y., Kallin, E.M., and Zhang, Y. (2009). Role of Jhdm2a in regulating metabolic gene expression and obesity resistance. Nature *458*, 757–761.

Yamamizu, K., Fujihara, M., Tachibana, M., Katayama, S., Takahashi, A., Hara, E., Imai, H., Shinkai, Y., and Yamashita, J.K. (2012). Protein kinase A determines timing of early differentiation through epigenetic regulation with G9a. Cell Stem Cell *10*, 759–770.

Yamane, K., Toumazou, C., Tsukada, Y., Erdjument-Bromage, H., Tempst, P., Wong, J., and Zhang, Y. (2006). JHDM2A, a JmjC-containing H3K9 demethylase, facilitates transcription activation by androgen receptor. Cell *125*, 483–495.

Stem Cell Reports, Volume *10*

Supplemental Information

Combined Loss of JMJD1A and JMJD1B Reveals Critical Roles for H3K9 Demethylation in the Maintenance of Embryonic Stem Cells and Early Embryogenesis

Shunsuke Kuroki, Yuji Nakai, Ryo Maeda, Naoki Okashita, Mika Akiyoshi, Yutaro Yamaguchi, Satsuki Kitano, Hitoshi Miyachi, Ryuichiro Nakato, Kenji Ichiyanagi, Katsuhiko Shirahige, Hiroshi Kimura, Yoichi Shinkai, and Makoto Tachibana

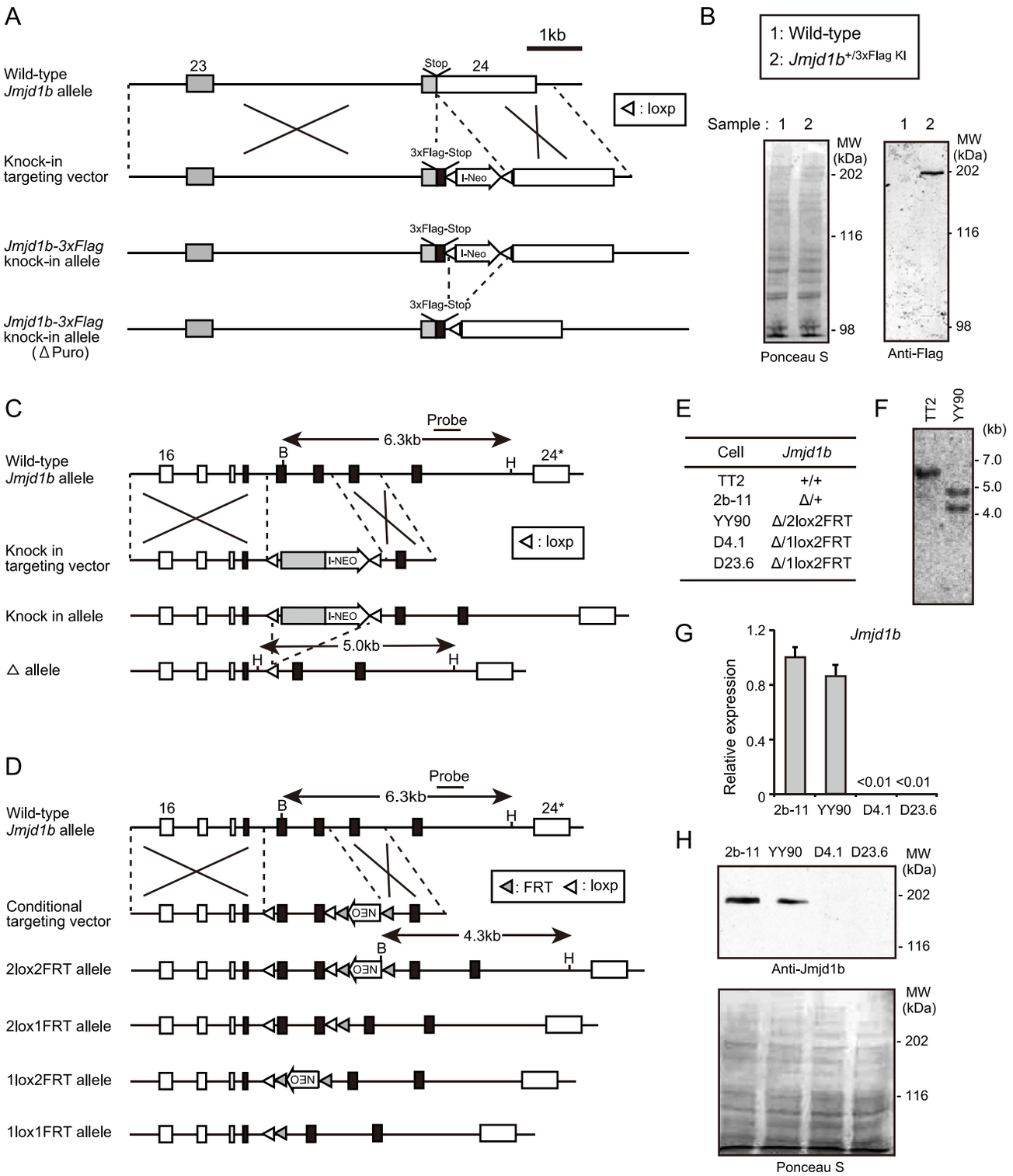

Figure S1. Generation of *Jmjd1b*$^{\text{Flag-KI}}$ Mouse and *Jmjd1b*-Deficient Mouse, Related to Figures 1, 2, and 5.
(A) Targeting strategy for generating *Jmjd1b*$^{\text{Flag-KI}}$ allele. Grey box indicates the coding region of *Jmjd1b*. The knock-in targeting vector involves DNA sequences encoding a triple Flag epitope tag and IRES-Neo, which are inserted at the 5' end of the termination codon in JMJD1B. (B) Immunoblot analysis of *Jmjd1b*$^{+/\text{Flag-KI}}$ ES cells. Whole cell extracts were prepared from the indicated ES cells, separated by SDS-PAGE, and then immunoblotted with anti-FLAG antibody. (C, D) Targeting strategy for generation of *Jmjd1b*$^{\Delta}$ allele (C) and *Jmjd1b*-conditional mutant allele (D). Grey box indicates the protein-coding region of *Jmjd1b* cDNA corresponding to exons 20-24. The targeting vectors were constructed by BAC recombineering technique using a BAC clone RP23-184N15. (E) List of established ES cell lines and their genotypes. (F) Southern blot analysis of wild-type and *Jmjd1b*$^{\Delta/2\text{lox2FRT}}$ ES cells. Genomic DNA was digested with *Hind*III and *Bam*HI, transferred to nylon membrane, and hybridized with a probe as shown in C and D. (G) Expression levels of *Jmjd1b* in the indicated cells were determined by quantitative RT-PCR analysis. Data were normalized to the expression levels of *Gapdh*. Data are presented as mean ± SD (n=3 independent experiments). (H) Whole cell extracts of the indicated cells were separated and immunoblotted with anti-JMJD1B antibodies. Pouceau S staining was used for confirmation of equal protein loading.

A

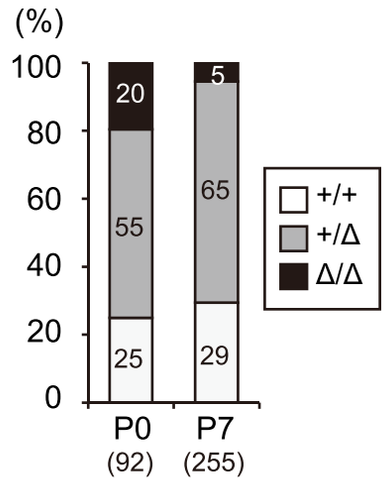

B

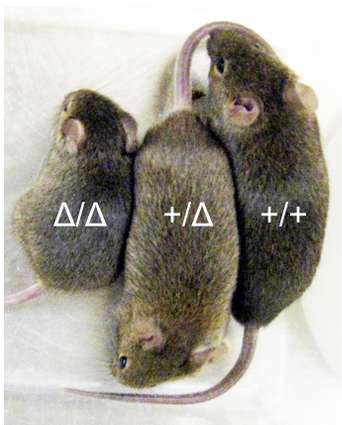

C

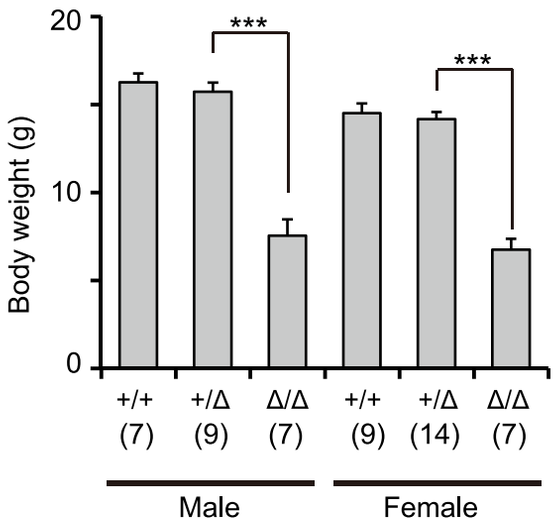

D

Jmjd1a :	+/+			+/Δ			Δ/Δ			
Jmjd1b :	+/+	+/Δ	Δ/Δ	+/+	+/Δ	Δ/Δ	+/+	+/Δ	Δ/Δ	Total
	10	23	10	16	36	4*	8	2*	0	109
Expected	6	12	6	12	25	12	6	12	6	

*All animals were stillborn.

Figure S2. Phenotypic Analysis of *Jmjd1b*-Deficient Mouse and *Jmjd1a*/*Jmjd1b*-Double Deficient Mouse, Related to Figure 1.

(A) *Jmjd1b*$^{+/\Delta}$ males and *Jmjd1b*$^{+/\Delta}$ females were crossed, and the resultant offspring were genotyped. The percentage of animals with the indicated genotypes is shown in the bar graph. *Jmjd1b*$^{\Delta/\Delta}$ mice were born at nearly the expected Mendelian ratio (P0), but most of them died within a week after birth (P7). The numbers of examined mice are shown in parenthesis. (B) Appearance of 6-week old littermate mice of *Jmjd1b* mutant mice. (C) The body weight of *Jmjd1b* mutant mice at 4-month-old age. The numbers of mice examined are shown in parenthesis. Data are presented as mean ± SD. ***P<0.001 (Student's test) (D) Genotype of newborn pups by mating *Jmjd1a*$^{+/\Delta}$; *Jmjd1b*$^{+/\Delta}$ males and females.

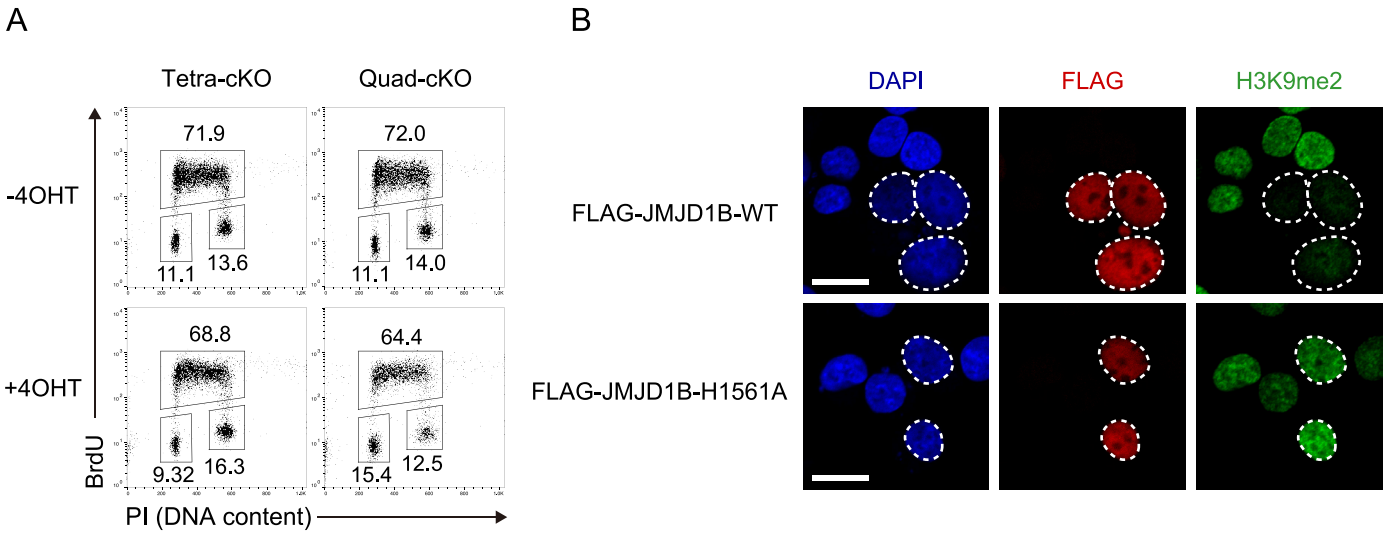

Figure S3. Phenotypic Analysis of JMJD1A/JMJD1B-Depleted ES cells, Related to Figure 2.
(A) Cell cycle analysis was conducted using 4OHT-treated Quad-cKO cells by measuring bromodeoxyuridine (BrdU) incorporation and the DNA contents. 4OHT treatment did not appear to have a profound effect on cell cycle progression in both Quad-cKO and Tetra-cKO cell lines. (B) Expression vectors for FLAG-tagged wild-type JMJD1B (upper) and mutant JMJD1B with H1561A mutation (bottom) were introduced into HEK293T cells. 2 days after introduction, cells were co-stained with anti-FLAG antibody (red) and anti-H3K9me2 antibody (green). Nuclei were counterstained with DAPI (blue). Scale bars, 20μm.

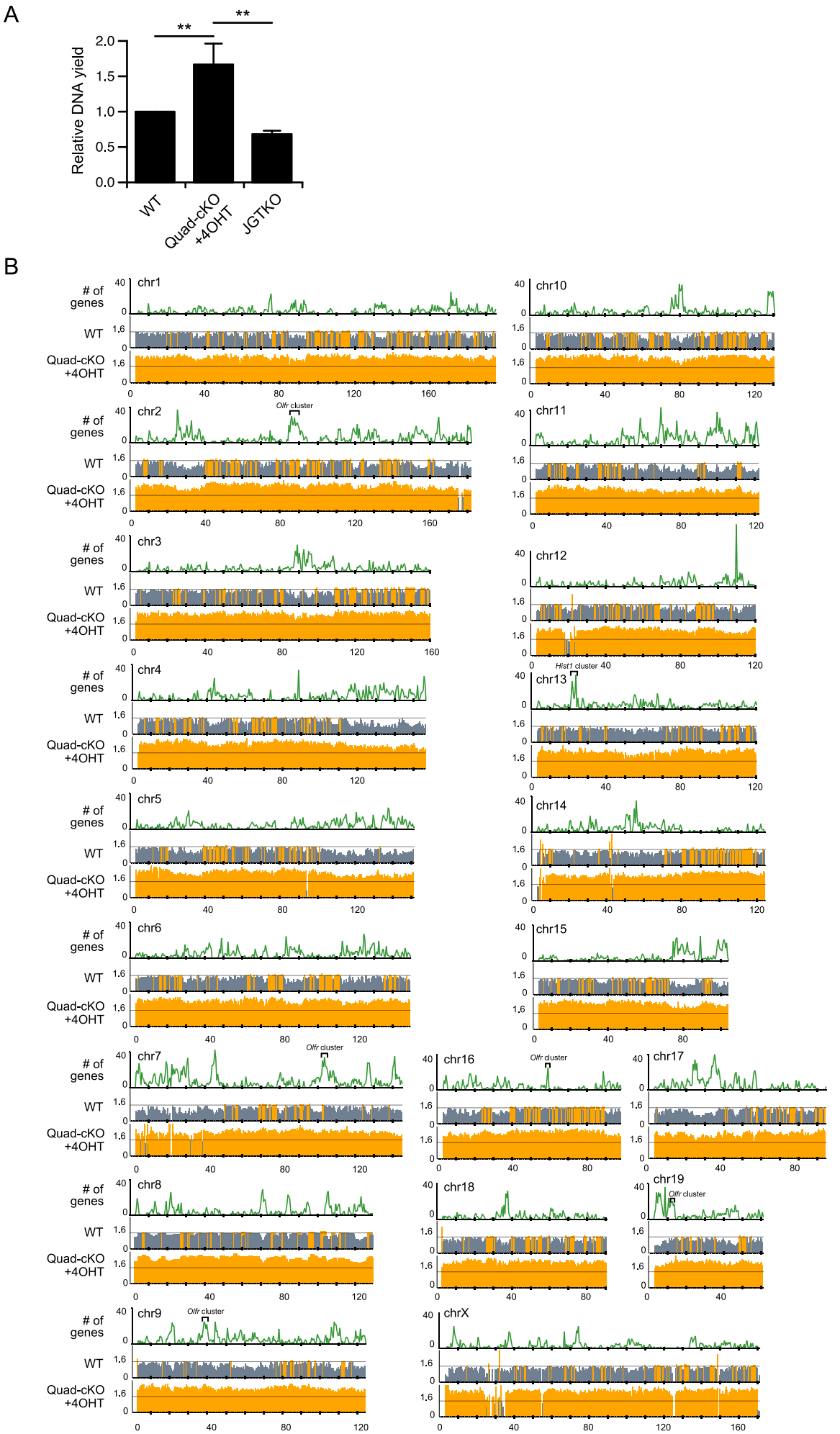
A
Relative DNA yield
2.0
1.5
1.0
0.5
0.0
**
**
WT
Quad-cKO +4OHT
JGTKO
B
# of genes
WT
Quad-cKO +4OHT
chr1
chr2
chr3
chr4
chr5
chr6
chr7
chr8
chr9
chr10
chr11
chr12
chr13
chr14
chr15
chr16
chr17
chr18
chr19
chrX
Olfr cluster
Hist1 cluster

Figure S4. ChIP Analysis of JMJD1A/JMJD1B-Depleted Cells with Anti-H3K9me2 Antibody, Related to Figure 4.

(A) Mononucleosomes were prepared from 2×10^5 ES cells of the indicated genotypes and subjected to native ChIP analysis with anti-H3K9me2 antibody. DNA was purified from immunеprecipitated chromatin and then subjected to quantification. DNA collected form wild-type cells was assumed as 1 for data normalization. Data are presented as mean ± SD (n=3 independent experiments). $^{**}P < 0.01$ (One-way ANOVA and Tukey HSD test). (B) Distribution profiles of H3K9me2 in chromosomes. The upper panel shows the number (#) of mm10 refseq genes smoothed with a 500 kb width. The middle and lower panels represent the ratios of normalized read density between ChIP and whole cell lysate (Input) samples (ChIP/Input) in wild-type (WT) and JMJD1A/JMJD1B-depleted cells (Quad-cKO+4OHT), respectively. The ratio of ChIP/Input > 1.6 are shown in orange. Several gene clusters, which had escaped from JMJD1A/JMJD1B-mediated H3K9 demethylation, are seen on the top panels.

A

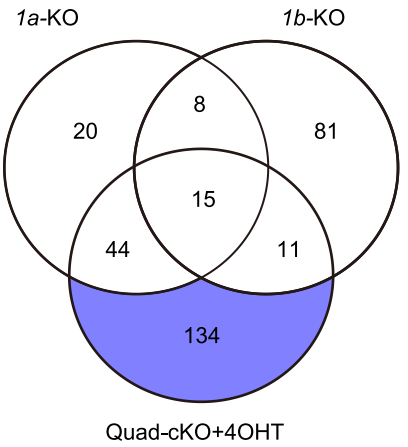

B

GO	Term	*p*-value
GO:0006730	one-carbon metabolic process	8.25×10^{-4}
GO:0030968	endoplasmic reticulum unfolded protein response	2.95×10^{-3}
GO:0007566	embryo implantation	5.54×10^{-3}
GO:0008152	metabolic process	6.58×10^{-3}
GO:0008652	cellular amino acid biosynthetic process	9.69×10^{-3}

C

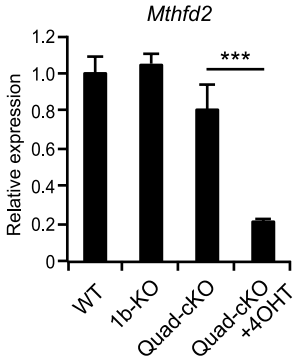

D

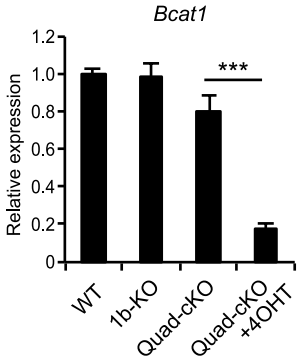

E

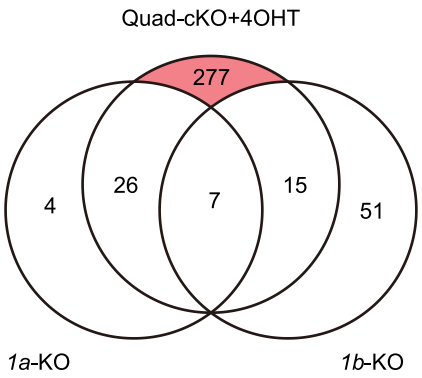

F

GO	Term	*p*-value
GO:0007286	spermatid development	7.47×10^{-11}
GO:0035458	cellular response to interferon-beta	1.27×10^{-6}
GO:0045596	negative regulation of cell differentiation	1.76×10^{-4}
GO:0008284	positive regulation of cell proliferation	5.16×10^{-4}
GO:0060333	interferon-gamma-mediated signaling pathway	1.10×10^{-3}
GO:0043066	negative regulation of apoptotic process	2.16×10^{-3}
GO:0086073	bundle of His cell-Purkinje myocyte adhesion involved in cell communication	2.71×10^{-3}
GO:0010833	telomere maintenance via telomere lengthening	4.97×10^{-3}
GO:0098911	regulation of ventricular cardiac muscle cell action potential	6.33×10^{-3}
GO:0044406	adhesion of symbiont to host	6.33×10^{-3}
GO:0086091	regulation of heart rate by cardiac conduction	6.48×10^{-3}
GO:0005975	carbohydrate metabolic process	7.69×10^{-3}
GO:0042832	defense response to protozoan	7.87×10^{-3}
GO:0007569	cell aging	7.87×10^{-3}
GO:0007129	synapsis	7.87×10^{-3}

Figure S5. Gene Ontology Analysis for Genes Regulated by JMJD1A and JMJD1B, Related to Figure 5.
(A) The number of genes whose expression was reduced by the depletion of JMJD1A, JMJD1B, or both is shown. Venn diagram indicates down-regulation of 134 genes in JMJD1A/JMJD1B-depleted cells. (B) Significantly enriched GO terms ($p < 0.01$) in 134 down-regulated genes. (C, D) RT-qPCR analysis of *Mthfd2* (methylenetetrahydrofolate dehydrogenase 2) and *Bcat1* (branched-chain amino acid transaminase 1). Both these genes were selected from the group of 134 down-regulated genes in JMJD1A/JMJD1B-depleted cells. MTHFD2 and BCAT1 are the key enzymes for one-carbon metabolism and amino acid catabolism, respectively. The expression levels of *Mthfd2* (C) and *Bcat1* (D) were drastically reduced due to the double mutation, but not single mutation, indicating that JMJD1A and JMJD1B redundantly activate these genes. Data are presented as mean ± SD (n=3 independent experiments). ***$P < 0.001$ (Student's *t* test). (E) The number of genes whose expression was up-regulated by the depletion of JMJD1A, JMJD1B, or both is summarized. Venn diagram indicates 277 genes up-regulated genes in JMJD1A/JMJD1B-depleted cells. (F) Significantly enriched GO terms ($p < 0.01$) in the 277 genes up-regulated by JMJD1A and JMJD1B in a redundant manner.

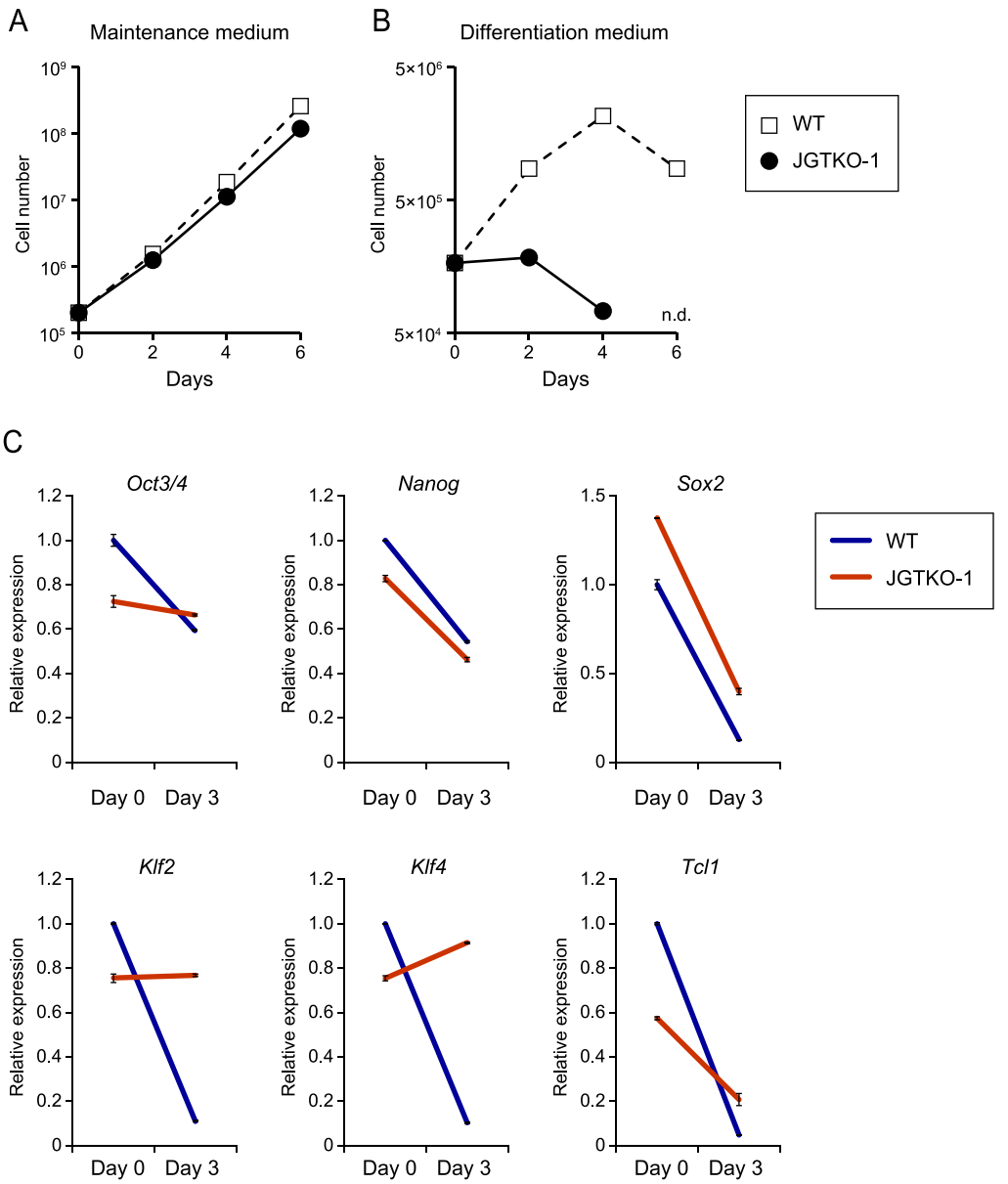

Figure S6. JMJD1A/JMJD1B- And G9A-Mediated H3K9 Methylation Tuning Is Important for ES Cell Differentiation, Related to Figure 6 and 7.

(A, B) Growth potential of JMJD1A/JMJD1B- and G9A-triple knock-out cells. JMJD1A/JMJD1B/G9A-triple deficient JGTKO-1 line was cultured in the maintenance medium (A) or in a differentiating medium without leukemia inhibitory factor (B; see Materials and Methods). (C) Perturbed transcriptional regulation of pluripotency-associated genes in JMJD1A/JMJD1B/G9A triple-deficient JGTKO-1 line under differentiating condition. Cells were cultured in the differentiation medium for 3 days, and mRNA expression of the indicated genes was analyzed using RT-qPCR. Values of gene expression in wild-type cells were considered as 1 for data normalization. Representative data are presented from n=3 independent experiments. Error bars indicate mean ± SD derived from technical replicates..

Table S1. Primer List Used in This Study

Primer name	Application	Sequence (5'->3')
2B-65420F	Probe synthesis for Southern blot analysis	AGGAAGCTGGCAGACCAGTA
2B-65900R		CGTTCTTCACCGACTTCCTC
Gapdh RT-PCR F	RT-qPCR	ATGAATACGGCTACAGCAACAGG
Gapdh RT-PCR R		CTCTTGCTCAGTGTCCTTGCTG
Jmjd1b 62315F	RT-qPCR	GGAGATGCTGATGAGGTGACCAAGC
Jmjd1b 62415R		GGATCTTCTCTGCATCCTTCGCTGC
2B-60841F	Detection of *Jmjd1b*+ and *Jmjd1b*! alleles	GCACCAAGCACTGCCACGGAGCTGA
2B-63090R		GATTAAAGGCTTGCACTACTAGACTCACTG
2B-61290R		ACCAGGTGCCGCTACATGAAGCTGG
TSGA-G2150F	Detection of *Jmjd1a*+ and *Jmjd1a*! alleles	CATACTGGTCTCCAGGAGCCAGAGG
TSGA-G1475R		GAACTGCACCATTAGCTGTCACTTCC
TSGA-G6540F		TCAGACAGTCCTGGGATCAGACACAC
Oct4-F	RT-qPCR	TGAGAACCGTGTGAGGTGGAGTCTG
Oct4-R		AAGCTGATTGGCGATGTGAGTGATC
Ccnd1-F	RT-qPCR	CGAAGAGGAGGTCTTCCCGCTGGCC
Ccnd1-R		CCCAGCAGCTGCAGGCGGCTCTTCT
Nnog-F	RT-qPCR	TTTGGAGGTGAATTTGGAAGC
Nanog-R		TCACCTGGTGGAGTCACAGAG
Sox2-F	RT-qPCR	CTTGCTGGGTTTTGATTCTGC
Sox2-R		AAGACCACGAAAACGGTCTTG
Klf2-F	RT-qPCR	CCCCAGGAAAGAAGACAGGAG
Klf2-R		AGGCATTTCTCACAAGGCATC
Klf4-F	RT-qPCR	GACCAGGATTCCCTTGAATTG
Klf4-R		ACCAAGCACCATCATTTAGGC
Tcl1-F	RT-qPCR	TGGCCTCACTAGAACAAGAGG
Tcl1-R		CTCGGTCAAGGATGGAAGC
Brachyury-F	RT-qPCR	AAGGACAGAGAGACGGCTGTG
Brachyury-R		AAAGTAGGACAGGGGGTGGAC
Fgf5-F	RT-qPCR	ATGAGTGCATCTGCTCTGCTC
Fgf5-R		CGTCTGTGGTTTCTGTTGAGG
Gata4-F	RT-qPCR	CTCCAGCCTGAACATCTACCC
Gata4-R		TGTGTGTGAAGGGGTGAAAAG
Mthfd2 #2 Fwd	RT-qPCR	AGAACCTCACCAGGATGCCCATCAG
Mthfd2 #2 Rev		TTCAGCATCCACTCTCGGTGTGAGG
Bcat1-e1 F	RT-qPCR	TGAGTTTAAGGTATGTGAGAGACAC
Bcat1-e1 R		CTGTCCCTGAGCCGAACATCTCCTT
Oct4-p-F	ChIP-qPCR	ATGGTGTAGAGCCTCTAAACTCTGG
Oct4-p-R		GTGAACCCAGTATTTCAGCCCATGT
Ccnd1-p1-F	ChIP-qPCR	CATTGCTTAGAAATCCCAGCGTCCC
Ccnd1-p1-R		CTCGTCTGGCATCTTCGGGTGTTAC

Supplemental Experimental Procedures

Antibodies

The poly histidine tag-fused polypeptide corresponding to amino acids 518K to 647H of JMJD1B (NP 001074725) was bacterially expressed, purified, and then used to immunize a rabbit. Rabbit polyclonal antibodies used against JMJD1A have been described previously (Tachibana et al., 2007). The other antibodies used in this study were anti-FLAG (M2, Sigma), anti-OCT3/4 (Abcam, ab19857), anti-β-actin (Wako, 013-24553), anti-G9A (Perseus Proteomics, #8620), anti-tubulin (Merck Millipore, CP06), anti-BrdU (BD Biosciences, 347580) and a panel of mouse antibodies against H3K9me1 (clone 2F7a), H3K9me2 (clone 6D11), and H3K9me3 (clone 2F3) (Kimura et al., 2008). For ChIP analysis, anti-H3K9me2 (Abcam, Ab1220) was used.

Immunofluorescence analysis

The embryos were fixed in 4% paraformaldehyde for 2 h at 4°C. For immunohistological analysis, the embryos were embedded in paraffin and cut into 4-μm-thick sections using a standard protocol. The sections were deparaffinized, rehydrated, and heated at 105°C for 5 min in10 mM citric acid buffer (pH 6.0). For whole-mount immunostaining, fixed embryos were permeabilized with PBS containing 0.5% Triton-X100 and 1% BSA for 20 min at RT. For immunocytochemistry, ES cells were cultured in slide chambers (ibidi) in the presence of 4OHT (800 nM) for 4 days. The cells were fixed in 2% PFA for 15 min, followed by permeabilization with 0.2% Triton-X100 for 30 min at RT.
For immunofluorescence staining, samples were blocked with TBS containing 2% skim milk and 0.1% Triton X-100 for 1 h, and then, incubated with the primary antibodies overnight at 4°C. This was followed by incubation with Alexa-conjugated secondary antibodies for 1 h and counterstaining with DAPI (1 μg/ml). The samples were mounted in Vectashield (Vector) and analyzed by confocal scanning microscopy (LSM700, Carl Zeiss). For whole-mount immunofluorescence analysis, Z-stack images (1 μm each) were collected and the maximum projections were processed using Zen 2011 imaging software (Carl Zeiss). Fluorescence intensity was measured using NIH ImageJ software.

Generation of *Jmjd1b*-deficient mice

The *Jmjd1b* knock-in targeting vector was constructed by the bacterial artificial chromosome (BAC) recombineering technique (Copeland et al., 2001) (Supplemental Fig. S1C), and then introduced into the ES cell line TT2. Homologous recombinant clones were identified by Southern blot analysis (Supplemental Fig. S1F). Chimeric males derived from two independent ES clones were used to generate F1 offspring bearing the mutant alleles, which were further crossed with *Pgk-2 Cre* transgenic mice (Ando et al., 2000), in order to generate the $Jmjd1b^{\Delta}$ allele. The resultant $Jmjd1b^{\Delta/+}$ females and males were crossed to generate *Jmjd1b*-deficient mice and embryos. All animal experiments were performed under the animal ethical guidelines of Tokushima University (experiment number 14108, approved by The Ethics Committee of Tokushima University for Animal Research) and Kyoto University (experiment number A12-6-2, approved by Animal Experimentation Committee of Kyoto University).

Generation of *Jmjd1b*-deficient ES cells

Jmjd1b-conditional targeting vector was constructed using the BAC recombineering technique (Supplemental Fig. S1D) and introduced into the $Jmjd1b^{\Delta/+}$ ES cell line 2b-11. Homologous recombination was confirmed by Southern blot analysis with the aforementioned probe. The homologous recombinant ES cell line YY90 (genotype: $Jmjd1b^{\Delta/2lox2FRT}$) was used for further evaluation. The

Jmjd1b-deficient ES cell lines, D23.6 and D4.1 (genotype: $Jmjd1b^{\Delta/1lox2FRT}$), were established from a pool of YY90 cells infected with Cre-expressing recombinant adenoviruses.

Generation of ES cells carrying the *Jmjd1a* knockout- and *Jmjd1b*-conditional knockout alleles

Jmjd1b conditional targeting vector was introduced into the *Jmjd1a*-deficient ES line 31-1 (Inagaki et al., 2009). The expression plasmid for MerCreMer was then introduced into the recombinant ES cell lines #117 and #131 (genotype: $Jmjd1a^{\Delta/\Delta}$; $Jmjd1b^{2lox1FRT/2lox2FRT}$).

Generation of ES cells lacking JMJD1A, JMJD1B, and G9A

G9a conditional targeting vector was introduced into the ES line #131. Homozygous mutants for the *G9a*-conditional knockout allele were successfully obtained when heterozygous mutants were cultured with 2.4 mg/ml G418 (3 of 40 clones). The plasmid for MerCreMer expression was introduced into the ES line 131-30-1 (genotype: $Jmjd1a^{\Delta/\Delta}$; $Jmjd1b^{2lox1FRT/2lox2FRT}$; $G9a^{2lox/2lox}$).

TUNEL assay

TdT-mediated UTP nick end labeling (TUNEL) was performed against the immunostained whole-mount embryos using the In Situ Cell Death Detection Kit (Roche) according to manufacturer's instructions. Images were collected and analyzed with the LSM700 microscope and Zen 2011 imaging software (Zeiss), respectively.

FACS analysis

ES cells were cultured in the presence of 4OHT (800 nM) for 2 or 4 days. For the cell death analysis, PI/annexin-V staining was performed using the MEBCYTO Apoptosis assay kit (MBL) according to the manufacturer's protocol. For the cell cycle analysis, deoxyuridine (BrdU) and PI staining was performed as described previously (Iwano et al., 2004) with some modifications. Briefly, ES cells were labeled with 20 μM BrdU for 30 min and fixed in 70% ethanol. The fixed cells were treated with 2 N HCl, washed in 1% BSA/PBS, and stained with anti-BrdU antibody. After washing, the cells were incubated with Alexa488-conjugated secondary antibody. Subsequently, the cells were incubated with RNase; PI (10 μg/ml) was added just before the analysis. The flow cytometric analysis was performed with a FACS Canto II flow cytometer (BD Biosciences).

ES cell culture

ES cells were maintained in Dulbecco's modified Eagle's medium, containing 10% knockout SR (Invitrogen), 1% fetal calf serum, and leukemia-inhibiting factor (10^3 U/ml). To delete the conditional allele of *Jmjd1b*, ES cells were cultured in the presence of 800 nM OHT. In the differentiation experiments of ES cells, cells were cultured in Dulbecco's modified Eagle's medium containing 10% fetal calf serum without leukemia-inhibiting factor.

Genotyping

Genotyping of the *Jmjd1a*-deficient and *Jmjd1b*-deficient mice/embryos was performed by PCR using the primers described in Supplemental Table S1.

Immunoblot analysis

Whole lysates of ES cells were fractionated by SDS electrophoresis and transferred to nitrocellulose membranes. The membranes were visualized with an enhanced chemiluminescence (ECL) kit (Perkin Elmer). The band intensities were quantified using the ImageJ software (National Institutes of Health).

ChIP analysis

Native ChIP of H3K9me2 was performed following a protocol described previously (Tachibana et al., 2008) with a slight modification. Briefly, 2 x 10^5 cells were suspended in 25 µl of 0.3 M sucrose-containing buffer 1 (60 mM KCl, 15 mM NaCl, 5 mM MgCl2, 0.1 mM EGTA, 0.5 mM DTT, 15 mM Tris-HCl pH 7.5, and protease inhibitor cocktail). The cells were then lysed following the addition of 0.3 M sucrose-containing buffer 1 (25 µl) with 0.8% NP40 on ice for 10 min; 1.2 M sucrose-containing buffer 1 (400 µl) was added and the chromatin was collected as pellets by centrifugation. The pellets were digested with micrococcal nuclease (0.05 U, Takara) in 10 µl of digestion buffer (0.32 M sucrose, 4 mM $MgCl_2$, 1 mM $CaCl_2$, 50 mM Tris-HCl pH 7.5) by vortexing at 37°C for 15 min; digestion was stopped with EDTA. The supernatant was obtained by centrifugation and incubated with anti-H3K9me2-conjugated magnetic beads (Dynabeads Protein G, Invitrogen) in 50 µl of incubation buffer (50 mM NaCl, 5 mM EDTA, 0.1% NP40, 20 mM Tris-HCl pH 7.5) at 4°C for 6 h. Then, DNA was extracted from the immune complex according to the standard protocol and quantified using Qubit ds DNA HS Assay Kit (Thermo Fisher Scientific), and then analyzed by real-time PCR. For ChIP of JMJD1A and FLAG-tagged JMJD1B, cross-link ChIP was performed following a protocol described previously (Kuroki et al., 2017).

ChIP-Seq analysis

DNA from input and Native ChIP fractions of H3K9me2 was processed and sequenced using the Illumina HiSeq-2500 system according to the manufacturer's instructions. In brief, the DNA was sheared to a mean size of ~150 bp by ultrasonication (Covaris), end-repaired, ligated to sequencing adapters, amplified, size-selected, and sequenced to generate single-end reads. Sequence reads were mapped to mouse mm10 genome using Bowtie2 (v 2.1.0) after trimming the first base from 5' end of reads (-5 1 option). Only uniquely mapped and non-redundant reads were used for further analysis. The mapped reads were processed and visualized using DROMPA (v 3.2.6) (Nakato et al., 2013). To compare WT and Quad-cKO and JGTKO ChIP-seq data, ChIP and input reads were normalized to the concentration of ChIPed DNA after normalization for read numbers (Supplemental Fig. S4 and S6). The processed reads were visualized using the GV (with -binsize 500000 option; to show the ratio of normalized read density between ChIP and input samples) and PC_ENRICH (with -binsize 5000 option; to show the normalized read density of ChIP and the corresponding input samples) commands in DROMPA. Down- and up-regulated genes were defined as genes having log2 fold change < -1 or > 1, respectively, in Quad-cKO + 4OHT versus WT. Plotting of averaged reads around gene bodies was performed using the PROFILE command in DROMPA based on the following parameters: -ptype 3 -stype 1 -binsize 5000.
ChIP-seq data from this study have been submitted to DDBJ Read Archive database (http://trace.ddbj.nig.ac.jp/dra/index_e.shtml) under accession number "DRA006496".

Microarray analysis

Total RNA was purified from ES cells with an RNeasy mini kit (Qiagen). DNA microarray analysis was performed according to the manufacturer's protocol. In brief, biotinylated cRNA was synthesized from 200 ng of total RNA and hybridized to an Affymetrix Mouse Genome 430 2.0 array. Affymetrix GeneChip Command Console software was used to reduce the array image to the intensity of each probe (CEL files). All microarray data are MIAME compliant and have been deposited in a MIAME-compliant database, the National Center for Biotechnology Information (NCBI) Gene Expression Omnibus

(http://www.ncbi.nlm.nih.gov/geo/, GEO Series accession number GSE98761), as detailed on the FGED Society website (http://fged.org/projects/miame/).
The CEL files were quantified with the factor analysis for robust microarray summarization (FARMS) (Hochreiter et al., 2006) using R (http://www.r-project) and Bioconductor (http://www.bioconductor.org/) (Gentleman et al., 2004). Hierarchical clustering was performed using the pvclust function (Suzuki and Shimodaira, 2006). The annotation file for Mouse Genome 430 2.0 Array was downloaded from the Affymetrix website (October 23, 2013, Mouse430_2.na34.annot.csv).

Supplemental Reference

Ando, H., Haruna, Y., Miyazaki, J., Okabe, M., and Nakanishi, Y. (2000). Spermatocyte-specific gene excision by targeted expression of Cre recombinase. Biochemical and biophysical research communications *272*, 125-128.

Copeland, N.G., Jenkins, N.A., and Court, D.L. (2001). Recombineering: a powerful new tool for mouse functional genomics. Nature reviews Genetics *2*, 769-779.

Gentleman, R.C., Carey, V.J., Bates, D.M., Bolstad, B., Dettling, M., Dudoit, S., Ellis, B., Gautier, L., Ge, Y., Gentry, J.*, et al.* (2004). Bioconductor: open software development for computational biology and bioinformatics. Genome Biol *5*, R80.

Hochreiter, S., Clevert, D.A., and Obermayer, K. (2006). A new summarization method for Affymetrix probe level data. Bioinformatics *22*, 943-949.

Inagaki, T., Tachibana, M., Magoori, K., Kudo, H., Tanaka, T., Okamura, M., Naito, M., Kodama, T., Shinkai, Y., and Sakai, J. (2009). Obesity and metabolic syndrome in histone demethylase JHDM2a-deficient mice. Genes Cells *14*, 991-1001.

Iwano, T., Tachibana, M., Reth, M., and Shinkai, Y. (2004). Importance of TRF1 for functional telomere structure. J Biol Chem *279*, 1442-1448.

Kimura, H., Hayashi-Takanaka, Y., Goto, Y., Takizawa, N., and Nozaki, N. (2008). The organization of histone H3 modifications as revealed by a panel of specific monoclonal antibodies. Cell Struct Funct *33*, 61-73.

Kuroki, S., Okashita, N., Baba, S., Maeda, R., Miyawaki, S., Yano, M., Yamaguchi, M., Kitano, S., Miyachi, H., Itoh, A.*, et al.* (2017). Rescuing the aberrant sex development of H3K9 demethylase Jmjd1a-deficient mice by modulating H3K9 methylation balance. PLoS Genet *13*, e1007034.

Nakato, R., Itoh, T., and Shirahige, K. (2013). DROMPA: easy-to-handle peak calling and visualization software for the computational analysis and validation of ChIP-seq data. Genes Cells *18*, 589-601.

Suzuki, R., and Shimodaira, H. (2006). Pvclust: an R package for assessing the uncertainty in hierarchical clustering. Bioinformatics *22*, 1540-1542.

Tachibana, M., Matsumura, Y., Fukuda, M., Kimura, H., and Shinkai, Y. (2008). G9a/GLP complexes independently mediate H3K9 and DNA methylation to silence transcription. The EMBO journal *27*, 2681-2690.

Tachibana, M., Nozaki, M., Takeda, N., and Shinkai, Y. (2007). Functional dynamics of H3K9 methylation during meiotic prophase progression. The EMBO journal *26*, 3346-3359.